JGP Journal of General Physiology

COMMUNICATION

Excitation–Contraction Coupling

Mice with R2509C-RYR1 mutation exhibit dysfunctional Ca^{2+} dynamics in primary skeletal myocytes

Yoshitaka Tsuboi[1,2*], Kotaro Oyama[3,4*], Fuyu Kobirumaki-Shimozawa[4], Takashi Murayama[5], Nagomi Kurebayashi[5], Toshiaki Tachibana[1], Yoshinobu Manome[1], Emi Kikuchi[1], Satoru Noguchi[6], Takayoshi Inoue[7], Yukiko U. Inoue[7], Ichizo Nishino[6], Shuichi Mori[8], Ryosuke Ishida[8], Hiroyuki Kagechika[8], Madoka Suzuki[9], Norio Fukuda[4], and Toshiko Yamazawa[1,2]

Type 1 ryanodine receptor (RYR1) is a Ca^{2+} release channel in the sarcoplasmic reticulum (SR) of the skeletal muscle and plays a critical role in excitation–contraction coupling. Mutations in *RYR1* cause severe muscle diseases, such as malignant hyperthermia, a disorder of Ca^{2+}-induced Ca^{2+} release (CICR) through RYR1 from the SR. We recently reported that volatile anesthetics induce malignant hyperthermia (MH)-like episodes through enhanced CICR in heterozygous R2509C-RYR1 mice. However, the characterization of Ca^{2+} dynamics has yet to be investigated in skeletal muscle cells from homozygous mice because these animals die in utero. In the present study, we generated primary cultured skeletal myocytes from R2509C-RYR1 mice. No differences in cellular morphology were detected between wild type (WT) and mutant myocytes. Spontaneous Ca^{2+} transients and cellular contractions occurred in WT and heterozygous myocytes, but not in homozygous myocytes. Electron microscopic observation revealed that the sarcomere length was shortened to ∼1.7 µm in homozygous myocytes, as compared to ∼2.2 and ∼2.3 µm in WT and heterozygous myocytes, respectively. Consistently, the resting intracellular Ca^{2+} concentration was higher in homozygous myocytes than in WT or heterozygous myocytes, which may be coupled with a reduced Ca^{2+} concentration in the SR. Finally, using infrared laser-based microheating, we found that heterozygous myocytes showed larger heat-induced Ca^{2+} transients than WT myocytes. Our findings suggest that the R2509C mutation in RYR1 causes dysfunctional Ca^{2+} dynamics in a mutant-gene dose-dependent manner in the skeletal muscles, in turn provoking MH-like episodes and embryonic lethality in heterozygous and homozygous mice, respectively.

Introduction

The skeletal muscle contracts when depolarization is transmitted to the dihydropyridine receptor in the T-tubule, and Ca^{2+} is released through type 1 ryanodine receptor (RYR1) from the sarcoplasmic reticulum (SR; Meissner, 1994; Iino, 1999; Rios, 2018; Woll and Van Petegem, 2022). RYR1 is a monomeric protein molecule consisting of ∼5,000 amino acids that form a tetramer; this protein functions as a giant Ca^{2+} release channel with Ca^{2+}-induced Ca^{2+} release (CICR) properties (Schneider, 1994; Endo, 2009; Rios, 2018). Mutations in RYR1 have been reported to induce severe muscle diseases, such as malignant hyperthermia (MH; MIM accession no. 145600) and central core disease (CCD; MIM accession no. 117000), the latter of which is characterized by muscle weakness (Treves et al., 2008; Allard, 2018; Jungbluth et al., 2018).

[1]Core Research Facilities, The Jikei University School of Medicine, Tokyo, Japan; [2]Department of Molecular Physiology, The Jikei University School of Medicine, Tokyo, Japan; [3]Quantum Beam Science Research Directorate, National Institutes for Quantum Science and Technology, Gunma, Japan; [4]Department of Cell Physiology, The Jikei University School of Medicine, Tokyo, Japan; [5]Department of Cellular and Molecular Pharmacology, Juntendo University Graduate School of Medicine, Tokyo, Japan; [6]Department of Neuromuscular Research, National Institute of Neuroscience, National Center of Neurology and Psychiatry, Tokyo, Japan; [7]Department of Biochemistry and Cellular Biology, National Institute of Neuroscience, National Center of Neurology and Psychiatry, Tokyo, Japan; [8]Institute of Biomaterials and Bioengineering, Tokyo Medical and Dental University, Tokyo, Japan; [9]Institute for Protein Research, Osaka University, Osaka, Japan.

*Y. Tsuboi and K. Oyama contributed equally to this paper. Correspondence to Toshiko Yamazawa: toshiko1998@jikei.ac.jp; Norio Fukuda: noriof@jikei.ac.jp; Madoka Suzuki: suzu_mado@protein.osaka-u.ac.jp

This work is part of a special issue on excitation–contraction coupling.

MH is induced by inhalational anesthetics, such as halothane and isoflurane, as well as by depolarizing muscle relaxants. Typical symptoms of MH are elevated body temperature (up to ~42°C) and enhanced skeletal muscle contraction. MH-related mutations in RYR1 are thought to cause massive Ca^{2+} release from the SR due to acceleration of CICR. MH is a relatively rare disease, occurring in only one in tens of thousands of cases of anesthesia; however, once it occurs, it can be fatal unless treated promptly (Sinha et al., 2017). It has also been reported that MH mutations in *RYR1* are involved in severe heat stroke (Wappler et al., 2001; Davis et al., 2002). Analyses of the *RYR1* gene in patients with MH and related muscle diseases have identified >300 different mutations located throughout the molecule, including in the N-terminal, central, and C-terminal regions (Lanner et al., 2010; Pancaroglu and Van Petegem, 2018).

The x-ray crystal structure of the RYR1 N-terminal region was resolved in 2010 (Tung et al., 2010). In 2015, three research groups (Efremov et al., 2015; Yan et al., 2015; Zalk et al., 2015) reported its protein structure at the near-atomic level using cryo-electron microscopy. In the following year, the structure of the channel in its open state was reported (des Georges et al., 2016), improving the understanding of its 3-D structure. To understand the detailed pathogenesis of MH, the structure and function of the mutants must also be comprehensively analyzed.

A heterologous expression system in HEK293 cells has been used for functional analysis of MH-related mutations in *RYR1* (Tong et al., 1997; Tong et al., 1999). We previously performed functional analysis using HEK293 cells overexpressing a disease mutant of *RYR1* that causes MH syndrome in humans (Murayama et al., 2015; Murayama et al., 2016; Yamazawa et al., 2020). We reported that the Y523S mutation in the N-terminal region (Murayama et al., 2015; Yamazawa et al., 2020) and R2508C mutation in the central region (Murayama et al., 2016) lead to extremely severe phenotypes that reduce the stability of the closed state of the channel, thereby causing Ca^{2+} leakage from the SR.

To fully understand the mechanisms by which MH occurs in humans, valid animal models are needed. Since the turn of the century, studies using knock-in/knockout mouse models with *RYR1* mutations, corresponding to human MH mutations, have been reported (Chelu et al., 2006; Yang et al., 2006; Yuen et al., 2012; Lopez et al., 2018). We previously generated an MH mouse model (R2509C-RYR1 mice) carrying a p.R2509C mutation in *RYR1* using the CRISPR/Cas9 system (Yamazawa et al., 2021). In R2509C-RYR1 heterozygous (R2509C-Het) mice, MH and MH-like episodes were induced by volatile anesthetics as well as by an increase in environmental temperature (Yamazawa et al., 2021). As in humans with MH, MH responses in R2509C-Het mice were characterized by sustained skeletal muscle contractions, resulting in hyperthermia, hyperventilation, rhabdomyolysis, and, ultimately, death. Additionally, R2509C-RYR1 homozygous (R2509C-Hom) mice died in utero (Yamazawa et al., 2021), as did knock-in homozygous mice with R163C (Yang et al., 2006) and Y524S (Chelu et al., 2006) RYR1 mutations. Therefore, no experiments on intracellular Ca^{2+} responses have been performed using skeletal muscle cells from R2509C-Hom mice. In the present study, we generated primary cultured skeletal myocytes to investigate Ca^{2+} dynamics in R2509C-Hom mice. We found that Ca^{2+} homeostasis was markedly disrupted in myocytes from R2509C-Hom mice, accompanied by sarcomere shortening.

Materials and methods

Animals

All animal experiments were performed in accordance with the regulations and guidelines of the Institutional Animal Care and approved by the Ethics Committees of The Jikei University School of Medicine. Mice were housed in isolator cages, fed with food and water ad libitum, and kept in a controlled environment with 12-h light/12-h dark cycles, 23–25°C temperature, and 50–60% relative humidity under specific pathogen-free conditions in the animal facilities of The Jikei University of Medicine. Homozygous mutant neonates were obtained by mating heterozygotes, and their littermates were used as controls. The genotypes of all neonates and embryos used in the experiments were determined using PCR analysis.

Preparation of skeletal muscle primary culture

Primary cultured myocytes at embryonic days 17–18 were prepared using a previously described procedure with some modifications (Rando and Blau, 1994; Yamazawa et al., 1996; Yamazawa et al., 1997). Briefly, the forelimbs and hindlimbs were removed from mice embryo, and the bones were dissected. The muscle was cut into small fragments and enzymatically dissociated with 2 mg/ml collagenase (Worthington Biochemical) and 2 mg/ml dispase (FUJIFILM Wako Pure Chemical Corporation) at 37°C for 40–50 min. The fragments were passed through a 40-µm cell strainer, and the suspension was subjected to low-speed centrifugation. The pellet was resuspended in Ham's Nutrient Mixture (F10), supplemented with 20% (v/v) FBS, penicillin (100 U/ml), streptomycin (100 U/ml), and 5 ng/ml recombinant human fibroblast growth factor-basic (Nacalai Tesque Inc.). Myoblasts were differentiated into myotubes/myocytes using Dulbecco's modified Eagle's medium (Nacalai Tesque Inc.) containing 2% horse serum. After 2–5 d of culture in differentiation medium, the myocytes were used in experiments. In optical heating experiments, 100 µM N-benzyl-N-nitroso-*p*-toluenesulfonamide (FUJIFILM Wako Pure Chemical Corporation) was added to HEPES-Krebs solution (140 mM NaCl, 5 mM KCl, 2 mM $CaCl_2$, 1 mM $MgCl_2$, 11 mM glucose, and 5 mM HEPES, pH 7.4) to suppress the movement of skeletal myocytes upon activation.

Preparation of single flexor digitorum brevis cells

Skeletal muscle cells isolated from mice were prepared based on a previously described procedure, with some modifications (Yamazawa et al., 2021). Briefly, WT and R2509C-Het mice (8–20 wk old) were anesthetized through intraperitoneal injection of an anesthetic mixture (0.75 mg/kg medetomidine, 4 mg/kg midazolam, and 5 mg/kg butorphanol) before euthanasia. Flexor digitorum brevis (FDB) muscles were dissected and incubated with 2 mg/ml collagenase (Worthington Biochemical) in the HEPES-Krebs solution containing 2 mg/ml BSA (A8806;

Merck) for 2 h at 37°C. Following incubation, single cells were separated by gentle trituration in HEPES-Krebs solution. Isolated single FDB fibers were seeded onto a laminin (Sigma-Aldrich)-coated or iMatrix-511 (T311; Takara Bio)-coated cover slip of a 35-mm glass-bottom dish. Next, 100 µM N-benzyl-N-nitroso-*p*-toluenesulfonamide, in HEPES-Krebs solution, was applied to suppress the movement of FDB fibers upon activation.

Ca^{2+} imaging

Cultured primary myocytes were incubated with 4 µM Cal-520-AM (AAT Bioquest) or fura-2-AM (Thermo Fisher Scientific) dye in HEPES-Krebs solution, containing 1 mg/ml BSA, for 30 min at room temperature (RT; 23–26°C). The cells were then washed thrice with HEPES-Krebs solution to remove excess dye; after 30 min of de-esterification, fluorescence images were obtained with a 20× objective lens (NA 0.75, UPlanSApo; Olympus) of an inverted microscope (DMI6000B; Leica) equipped with a complementary metal-oxide-semiconductor camera (ORCA-Flash4.0; Hamamatsu Photonics), at the rate of one frame every 0.5–2 s, using a MetaFluor v7 imaging system (Molecular Devices). The fluorescence wavelength was switched using a fluorescence filter exchanger (LAMBDA 10-3; Sutter Instrument). For Cal-520, it was excited at 480 ± 9 nm, and fluorescence was measured at 520 ± 14 nm. For fura-2, it was excited at alternating wavelengths of 340 (340 ± 13) nm and 380 (387 ± 6) nm, and the fluorescence was measured at 520 ± 14 nm for both wavelengths. Regions of interest corresponding to individual cells were selected and the mean fluorescence intensity (*F*) of each region of interest minus the background intensity was calculated for each frame.

We used the *F*340/*F*380 ratio (*R*; the value of *F* at an excitation wavelength of 340 nm divided by the value at an excitation wavelength of 380 nm) to estimate intracellular Ca^{2+} concentration ($[Ca^{2+}]_{cyt}$), as described previously (Murayama et al., 2016; Yamazawa et al., 2020).

The ratio (*R*) was converted to $[Ca^{2+}]_{cyt}$ using the following equations;

$$[Ca^{2+}]_{cyt} = K_d'(R - R_{min})/(R_{max} - R),$$
$$K_d' = K_d \times \beta$$

where K_d', R_{max}, and R_{min} are the apparent dissociation constant, maximal, and minimal *R* values, respectively, and β refers to the fluorescence intensity coefficient at 380 nm in the absence of Ca^{2+} to that in the presence of saturating Ca^{2+} (Grynkiewicz et al., 1985). K_d', R_{max}, and R_{min} were determined with the calibration solution (132 mM potassium methanesulfonate, 10 mM EGTA, 0–10 mM total calcium, 4 µM fura-2, 50 mg/ml BSA, and 20 mM PIPES, ionic strength 0.2, pH 7.0), which gave 0.1 nM–70 µM free Ca^{2+}. The calibration was carried out in the presence of BSA because fura-2 molecules reportedly bind to proteins in the cytoplasm, thereby changing the parameters of the dye (Konishi et al., 1988; Uto et al., 1991). The fura-2 solutions at various Ca^{2+} concentration were placed in a gap created between a coverslip and a glass bottom dish (800 µm thickness), and measurements were performed using the same apparatus as that used for Ca^{2+} measurements in cells. K_d', R_{max}, and R_{min} obtained in our apparatus were 10.8 µM, 33.6, and 0.35, respectively.

To measure the cell temperature, we used ERthermAC, a photostable fluorescent molecular thermometer that selectively targets the sarco-endoplasmic reticulum (SR/ER). Cultured primary myocytes were loaded with 4 µM Cal-520-AM and 200 nM ERthermAC in HEPES-Krebs solution, containing 1 mg/ml BSA, for 30 min at RT. ERthermAC was excited at 556 ± 10 nm, and fluorescence was measured at 617 ± 37 nm. Excitation light and emission filters for Cal-520 and ERthermAC were exchanged alternately.

Drugs were applied to the myocytes or FDB fibers using a homemade 6-channel puffing pipette (Yamazawa et al., 2020), which changed the solution surrounding the cells within ∼1 s.

Microscopy system for optical heating

The microscopy system used for optical heating has been described previously (Oyama et al., 2022). Briefly, confocal images were obtained using an inverted microscope (IX73; Olympus) equipped with a Nipkow confocal scanner unit (CSU-X1; Yokogawa Electric), a dichroic mirror (Di01-T405/488/561; Semrock), a 20× objective lens (UPlanSApo, NA = 0.75; Olympus), and an EM-CCD camera (iXon Ultra; Andor Technology). For imaging of Cal-520, a 488-nm laser light (Vortran Laser Technology) and an emission filter (FF01-520/35; Semrock) were used. The local temperature was increased using an infrared laser (KPS-STD-BT-RFL-1455-05-CO; Keopsys) with an IR-LEGO mini (SIGMAKOKI). The change in local temperature was calculated through thermal quenching of 10 µg/ml Alexa Fluor 555 conjugated to 10-kD dextran (D34679; Thermo Fisher Scientific) in HEPES-Krebs solution, as previously described (Oyama et al., 2015). The dye was excited using a 561-nm laser light (Cobolt), and the fluorescence was captured through an emission filter (FF01-617/73; Semrock). Microscopic experiments were performed at 24°C. To inhibit the activity of sarco- and endoplasmic reticulum Ca^{2+}-ATPase (SERCA), the myocytes were incubated in HEPES-Krebs solution containing 1 mg/ml BSA, 4 µM Cal-520AM, and 20 µM cyclopiazonic acid (CPA), for 30 min at 24–26°C, and then observed 60 min later in HEPES-Krebs solution containing 20 µM CPA.

Analyses for local heating

Microscopic images were analyzed using the ImageJ software (National Institutes of Health). The fluorescence intensity of Cal-520 was measured in an area of 139 µm^2. To minimize artifacts caused by movement and drifting focus due to contracture during heating, the area at the center of the cell was selected. The maximum changes in the relative intensity of Cal-520 ($\Delta F_{max}/F_0$) were calculated from the maximum and minimum F/F_0 for 5 s during heating, where *F* is the fluorescence intensity at an arbitrary time and F_0 is the averaged intensity for 1.2 s after the initiation of recording (i.e., 10 s before beginning the heating). If the maximum $F/F_0 - 1 > 1 -$ minimum F/F_0, then $\Delta F_{max}/F_0$ = maximum $F/F_0 - 1$. If the maximum $F/F_0 - 1 <$ $1 -$ minimum F/F_0, then $\Delta F_{max}/F_0$ = minimum $F/F_0 - 1$. The background intensity without excitation was subtracted.

To measure the change in local temperature, relative changes in Alexa Fluor 555 intensity were calculated as $\Delta F/F_0 = (F_{heating} - I_{back})/(F_{after} - I_{back})$, where $F_{heating}$ is the averaged intensity for

1 s at the end of the heating period, F_{after} is the averaged intensity for 1 s at ∼20 s after the end of heating, and I_{back} is the background intensity when the excitation light is turned off. The $\Delta F/F_0$ of Alexa Fluor 555 was converted to ΔT using the relationship between ΔT and $\Delta F/F_0$ (Oyama et al., 2015).

Immunohistochemistry

Primary cultured myocytes were fixed with 4% paraformaldehyde in PBS (T900; Takara Bio) and permeabilized with 0.3% Triton X-100 (X100; Sigma-Aldrich) in PBS. After rinsing with PBS, the cells were incubated with 2% BSA (01281-84; Nacalai Tesque Inc.) in PBS for 1 h at RT. For immunofluorescence staining, the cells were incubated overnight at 4°C with mouse–anti-myosin heavy chain antibody (MF20, 1:200; 14-6503-82; Thermo Fisher Scientific). After washing, the cells were incubated with Alexa Fluor 546 rabbit anti-mouse IgG (H+L; 1:1,000; A-11060; Thermo Fisher Scientific) and 4′,6-diamidino-2-phenylindole dye (1:1,000; 340-07971; Dojindo Laboratories) for 1 h at RT. Images of the primary cultured cells were captured using an LSM 880 confocal laser-scanning microscope (Carl Zeiss) equipped with a 20× objective (α Plan-Apochromat, NA 0.8; Carl Zeiss).

Western blotting

Myoblasts and myotubes were lysed with Pro-Prep protein extraction solution (iNtRON Biotechnology). The extracted proteins were separated on 3–15% polyacrylamide gels and transferred to PVDF membranes. Membranes were probed with the primary antibodies against myosin heavy chain (MHC; MF20; Thermo Fisher Scientific), RYR1 (F1; Santa Cruz Biotechnology), and GAPDH (6C5; Santa Cruz Biotechnology), followed by HRP-labeled anti-mouse IgG (04-18-18; Kirkegaard & Perry Laboratories). Positive bands were detected by chemiluminescence using ImmunoStar LD (FUJIFILM Wako Pure Chemical Corporation) as a substrate.

Transmission electron microscopy

Transmission electron microscopy (TEM) experiments were performed based on a previously described procedure (Yamazawa et al., 2016), with slight modifications. Briefly, primary skeletal muscle culture cells were fixed with 2% glutaraldehyde (Nacalai Tesque Inc.) in 0.1 M phosphate buffer for 1 h at 4°C and post-fixed with 1% osmium tetroxide (Nisshin EM Co., Ltd.) in the same buffer at 0°C for 30 min. The tissues were first dehydrated with a graded series of ethanol, further with 100% ethanol for 10 min three times, and embedded in Epok 812 (Oken). Sections of 60-nm thickness were cut with a diamond knife and mounted on grids. After staining with uranyl acetate and lead citrate, sections were examined using an H-7500 electron microscope (Hitachi) at 80 kV.

Statistical analysis

The unpaired Student's *t* test was used for comparisons between two groups. A one-way ANOVA followed by Tukey's test was performed to compare three or more groups. Multiple groups were compared using the Steel test. Mann–Whitney *U* test was used for comparisons of two independent samples. These tests were performed using Prism v7 and v9 (GraphPad Software, Inc.).

Online supplemental material

Fig. S1 shows the morphology of R2509C-Hom embryos. Fig. S2 shows the distribution of the lengths of A-band in WT and R2509C mutant primary myocytes. Fig. S3 shows spontaneous Ca^{2+} transients in WT and R2509C mutant primary myocytes. Fig. S4 shows the time-course of heat-induced Ca^{2+} release in WT and R2509C primary myocytes. Fig. S5 shows temperature measurement of the SR in WT and R2509C-Het FDB-isolated fibers. Fig. S6 shows ERthermAC staining in primary myocytes. Video 1 shows spontaneous contraction in WT myocytes. Video 2 shows spontaneous contraction in R2509C-Het myocytes. Video 3 shows spontaneous contraction in R2509C-Hom myocytes. Video S4 shows spontaneous Ca^{2+} transients in WT myocytes. Video 5 shows spontaneous Ca^{2+} transients in R2509C-Het myocytes. Video 6 shows spontaneous Ca^{2+} transients in R2509C-Hom myocytes.

Results

To characterize skeletal muscle cells from R2509C-Hom mice, primary cultures were prepared from WT and R2509C mouse skeletal muscle at embryonic days 17–18 (E17.5). We initially attempted to prepare primary-cultured skeletal muscle cells from neonatal R2509C mice; however, R2509C-Hom fetuses showed abnormal deaths between E17 and E19, with subcutaneous hemorrhage, subcutaneous effusion, and translucent skeletal muscles (see Fig. S1). These phenotypes were distinct from those in homozygous RYR1 knockout mice that have been reported to die in the neonatal period (*dyspedic* mice; see Takeshima et al., 1994). Indeed, we successfully prepared cultured skeletal muscle cells from neonatal *dyspedic* mice at E19.5 (Yamazawa et al., 1996).

Morphology of primary myocytes

Under the present culture conditions, primary myotubes/myocytes from WT and R2509C (R2509C-Het and R2509C-Hom) mice developed multiple nuclei within 3 d of differentiation induction (Fig. 1 A). The morphology of the cells was similar. Interestingly, primary myocytes from WT (Video 1) and R2509C-Het (Video 2) mice showed spontaneous contractions, whereas those from R2509C-Hom mice (Video 3) did not. Fluorescence immunostaining with anti-myosin heavy chain antibodies revealed a similar level of expression of MHC in WT, R2509C-Het, and R2509C-Hom myocytes (Fig. 1 B). Also, Fig. 1 C presents representative Western blots of MHC in WT, R2509C-Het, and R2509C-Hom myocytes up to 4 d after differentiation. There was no significant difference in average MHC expression levels between WT and R2509C myocytes from day 0–4 ($P > 0.05$). Therefore, it is unlikely that the absence of spontaneous contractions in R2509C-Hom myocytes occurred because of loss of myosin molecules.

The morphology of primary myocytes was further investigated after 3 d of differentiation using TEM (Figs. 2 and S2). Sarcomere structures were preserved with clear *Z*-lines in all

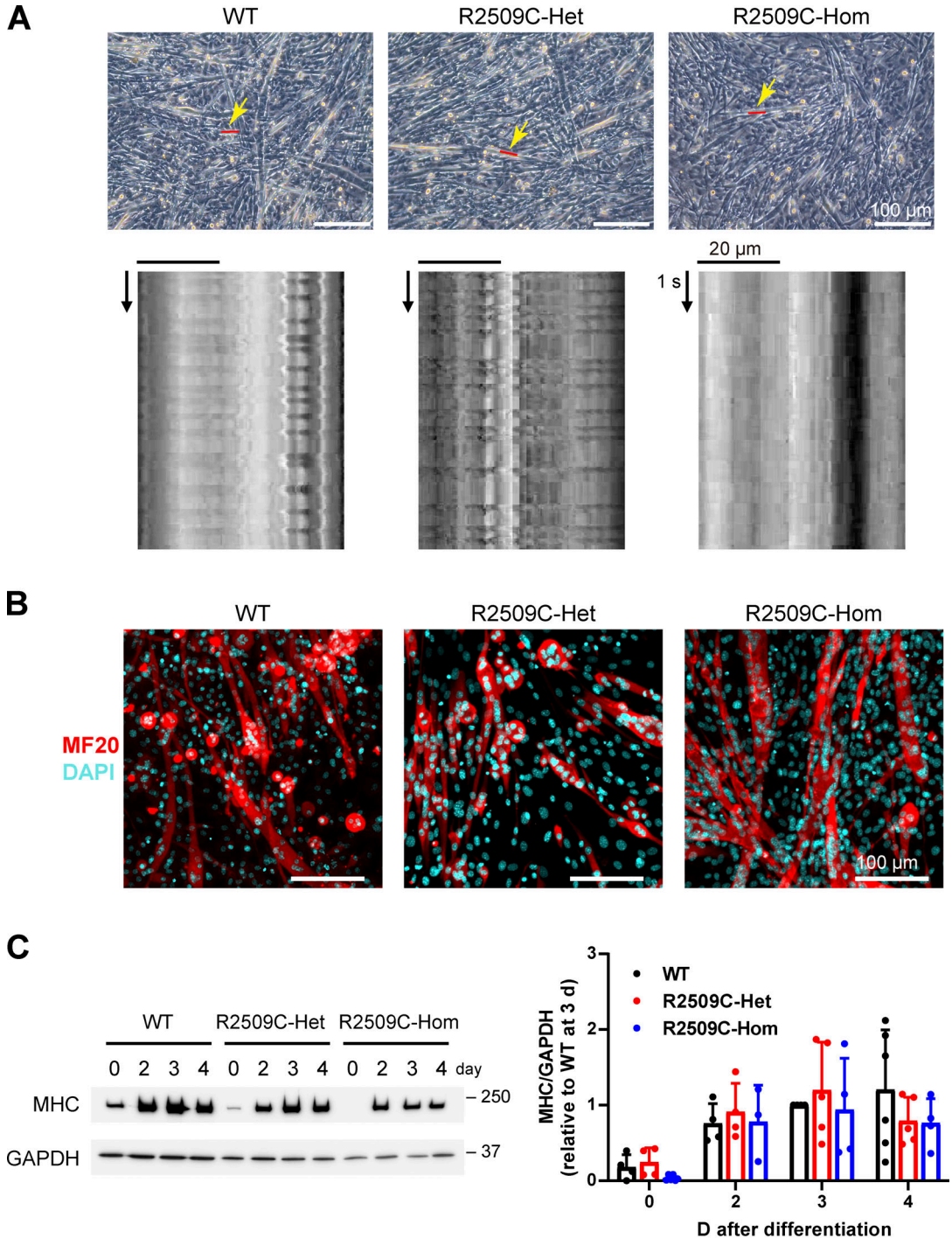

Figure 1. **Morphological characteristics of primary myocytes from WT and R2509C-RYR1 mice. (A)** Bright-field images of primary myocytes derived from WT (left) and R2509C-RYR1 mice (R2509C-Het [middle] and R2509C-Hom [right]) at 3 d after differentiation. Myocytes highlighted by red lines (also indicated by yellow arrows) are shown in the kymographs at the bottom (i.e., time-dependent changes in contrast). **(B)** Confocal images showing immunostained MHC (MF20) in red and nuclei stained with 4′,6-diamidino-2-phenylindole (DAPI) in cyan in primary myocytes. Left, middle, and right indicate WT, R2509C-Het, and R2509C-Hom myocytes, respectively. **(C)** Expression levels of MHC in myocytes. Left: Western blotting showing MHC and the loading control glyceraldehyde-3-phosphate dehydrogenase (GAPDH) in myocytes expressing WT, R2509C-Het (Het), and R2509C-Hom (Hom) myocytes. Molecular mass standards are shown on the right (kD). Right: Graph showing MHC/GAPDH analyzed from band intensities in Western blotting in WT, Het, and Hom. Data normalized by that of WT at day 3. Data are means ± SD (n = 4–6) and analyzed by two-way ANOVA with Tukey's test. Primary myocytes were cultured from three mice (N = 3) in each group.

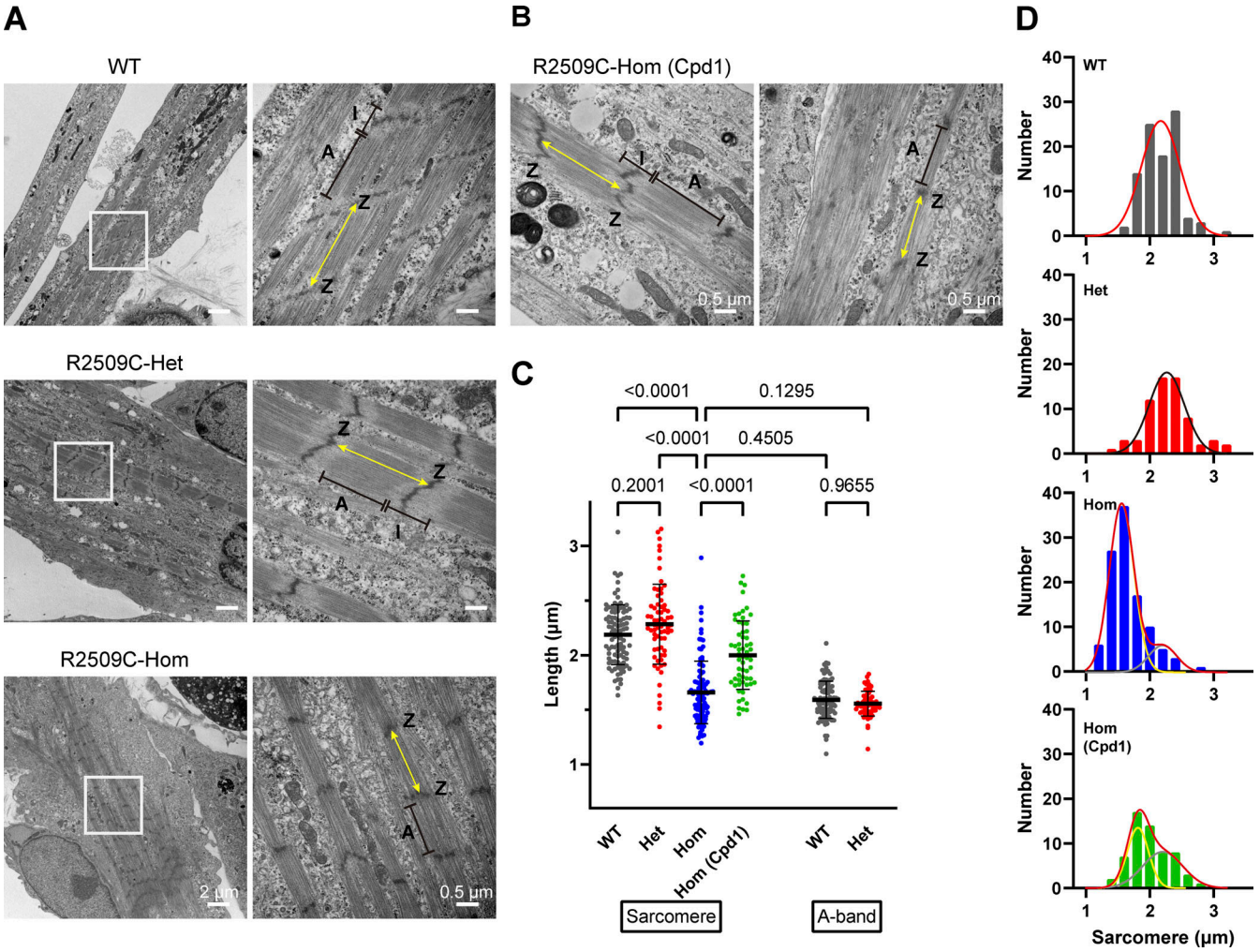

Figure 2. **Analysis of sarcomeres in WT and R2509C-RYR1 primary myocytes. (A)** TEM images of thin epoxy resin sections of primary cultured myocytes at 3 d after differentiation. Right panels show higher magnification of the area depicted by white-outlined squares in left panels. Sarcomere structure was preserved in WT (top), R2509C-Het (middle), and R2509C-Hom (bottom) myocytes. SL was measured as the distance between *Z*-lines (shown by yellow bidirectional arrows). A, I, and Z indicate the A-band, I-band, and Z-line, respectively. **(B)** TEM images of thin epoxy resin sections of primary cultured myocytes at 3 d after differentiation in the presence of Cpd1. Cpd1 was added at 2 µM from the onset of differentiation. Sarcomere structure was preserved in R2509C-Hom myocytes. SL was measured as the distance between *Z*-lines (shown by yellow bidirectional arrows). A, I, and Z indicate the A-band, I-band, and Z-line, respectively. **(C)** Graph showing SL in WT, R2509C-Het, R2509C-Hom, and R2509C-Hom (Cpd1) myocytes and the A-band length in WT and R2509C-Het myocytes. SL was significantly shorter in R2509C-Hom (1.7 ± 0.3 µm, *n* = 106 from 18 cells) myocytes than in WT (2.2 ± 0.3 µm, *n* = 95 from 15 cells) or R2509C-Het (2.3 ± 0.4 µm, *n* = 68 from 11 cells) myocytes. No significant difference was observed in the A-band length between groups (WT, 1.6 ± 0.1 µm, *n* = 95 from 15 cells; Het, 1.6 ± 0.1 µm, *n* = 68 from 11 cells; see Fig. S2). As indistinct I-bands were coupled with marked myofibrillar shortening in R2509C-Hom myocytes (see A), the A-band length was not measured to avoid errors. Treatment with Cpd1 significantly increased SL of R2509C-Hom (2.0 ± 0.3 µm, *n* = 60 from 14 cells) myocytes. Values are shown as mean ± SD. Statistical significance was determined using a one-way ANOVA with Tukey's test. Primary myocytes were cultured from three mice (*N* = 3) in each group. **(D)** Frequency histograms of SL in C. Gaussian fittings showed peaks at 2.2 and 2.3 µm for WT and R2509C-Het, respectively. Histograms for R2509C-Hom and R2509C-Hom+Cpd1 were analyzed by two Gaussians, with one of the peaks fixed at 2.2 µm. Shorter peaks for R2509C-Hom and R2509C-Hom+Cpd1 were 1.6 and 1.8 µm, respectively.

three types of primary myocytes (Fig. 2 A); however, the I-bands were not detected in R2509C-Hom myocytes, indicating the occurrence of sarcomere shortening. Indeed, the sarcomere length (SL) in R2509C-Hom myocytes (1.7 ± 0.3 µm) was significantly shorter than that in the WT (2.2 ± 0.3 µm) or R2509C-Het (2.3 ± 0.4 µm) myocytes ($P < 0.0001$ and 0.0001, respectively; Fig. 2 C). To confirm the contribution of RYR1 mutants to the marked shortening of SL in R2509C-Hom myocytes, we tested the effects of a novel RYR1 inhibitor, 6,7-(methylenedioxy)-1-octyl-4-quinolone-3-carboxylic acid (Cpd1; Mori et al., 2019; Yamazawa et al., 2021). Cpd1 (2 µM) was continuously applied to the culture media from the onset of differentiation. The SL in Cpd1-treated R2509C-Hom myocytes (2.0 ± 0.3 µm) was significantly longer than that in the R2509C-Hom myocytes (1.7 ± 0.3 µm; Fig. 2, B and C). To further investigate the distribution of SL, we have analyzed the histograms, as shown in Fig. 2 D. It is reasonable to assume that the distribution shows a single peak in WT, because myocytes are in the resting state. Indeed, the Gaussian fitting provided the mean ± SD as 2.2 ± 0.3 µm. The data in R2509C-Het were similarly fitted by a single Gaussian, providing the value as 2.3 ± 0.3 µm.

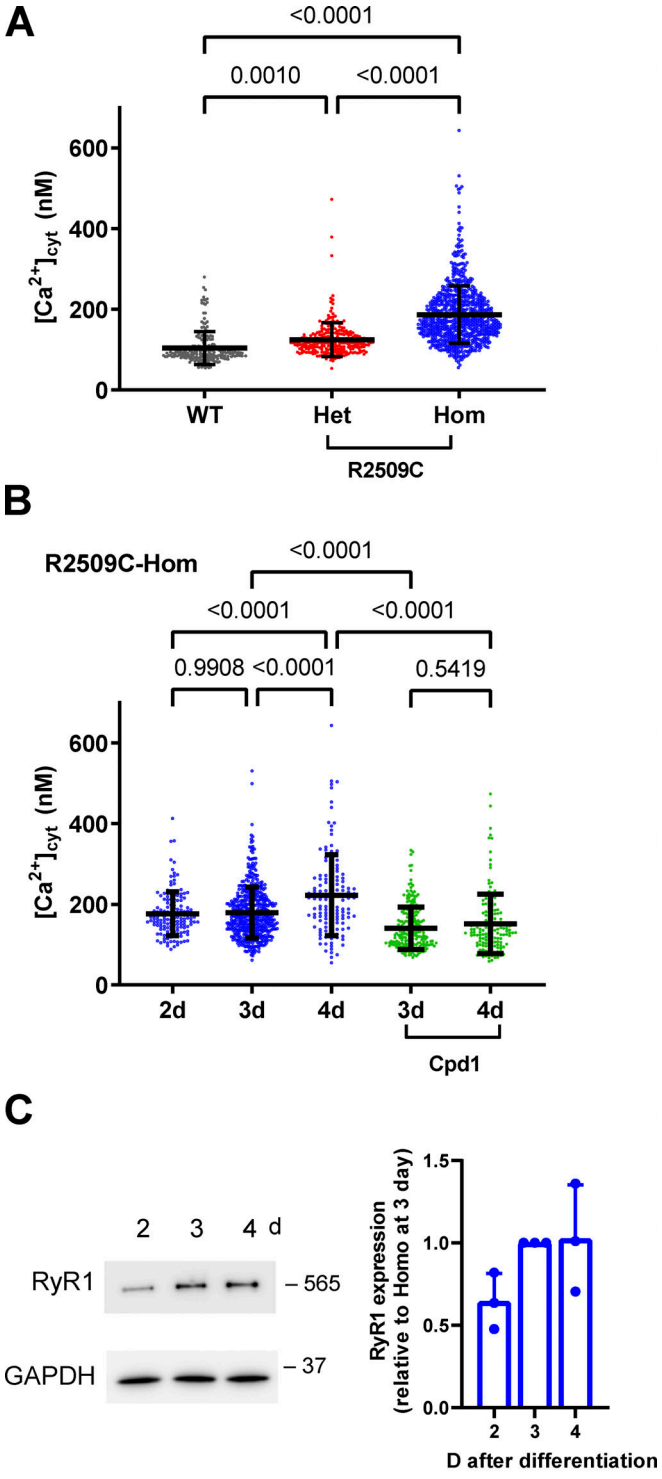

Figure 3. **Properties of resting $[Ca^{2+}]_{cyt}$ in WT and R2509C-RYR1 primary myocytes. (A)** Comparison of resting $[Ca^{2+}]_{cyt}$ in primary myocytes from WT (n = 205, N = 3), R2509C-Het (Het; n = 257, N = 3), and R2509C-Hom (Hom; n = 776, N = 4) mice. $[Ca^{2+}]_{cyt}$ was determined using fura-2. **(B)** Resting $[Ca^{2+}]_{cyt}$ in R2509C-Hom myocytes at 2 (176.6 ± 54.3 nM: n = 148, N = 3), 3 (179.5 ± 63.2 nM: n = 494, N = 4), and 4 (222.5 ± 100.3 nM: n = 134, N = 3) days after differentiation, and at 3 (140.6 ± 52.7 nM: n = 230, N = 3) and 4 (151.4 ± 73.5 nM: n = 151, N = 3) days after differentiation in the presence of Cpd1. Cpd1 was added at 2 µM at the onset of differentiation. Values are mean ± SD. Statistical significance was determined using one-way ANOVA with Tukey's test. **(C)** Expression levels of RYR1 in R2509C-Hom myocytes. Western blotting showing RYR1 and loading control GAPDH. Molecular mass standards are shown on the right (kD). In the graph on the right, data were normalized based on the values at day 3. Data are means ± SD (N = 3) and analyzed by one-way ANOVA with Tukey's test. "n" is the number of myocytes and "N" is the number of animals.

In contrast, R2509C-Hom and R2509C-Hom+Cpd1 were not fitted well by a single Gaussian (Fig. 2 D). Therefore, these data sets were analyzed using two Gaussians (discussed below in Discussion); one of the peak values was fixed at 2.2 µm in both groups, and the other peak values were derived as 1.6 ± 0.2 and 1.8 ± 0.2 µm in R2509C-Hom and R2509C-Hom+Cpd1, respectively.

Resting intracellular Ca^{2+} concentrations in R2509C primary myocytes

It was previously shown in MH mouse models that dyshomeostasis of $[Ca^{2+}]_{cyt}$ in skeletal myocytes is among the most common features of MH (Chelu et al., 2006; Yang et al., 2006). Therefore, we investigated whether and how Ca^{2+} transients are altered in R2509C-Hom myocytes. Fluorescence Ca^{2+} imaging showed that spontaneous Ca^{2+} transients occurred similarly as in WT (Fig. S3 A and Video 4) and R2509C-Het (Fig. S3 B and Video 5) myocytes but not in R2509C-Hom (Fig. S3 C and Video 6) myocytes (Fig. S3 D). We measured the resting intracellular Ca^{2+} concentration ($[Ca^{2+}]_{cyt}$) using fura-2, a ratiometric fluorescent Ca^{2+} indicator, in myocytes differentiated from primary myoblasts from WT and R2509C-RYR1 mice (at day 2–4 after the onset of differentiation). The average resting $[Ca^{2+}]_{cyt}$ in WT myocytes (103.7 ± 40.7 nM) was close to the reported value of ∼100 nM (see Harkins et al., 1993; Royer et al., 2008). Resting $[Ca^{2+}]_{cyt}$ was significantly higher in R2509C-Het myocytes (124.5 ± 42.0 nM), and highest in R2509C-Hom myocytes (186.4 ± 71.4 nM; Fig. 3 A and Table 1). Therefore, the data for R2509C-Hom myocytes were further analyzed by varying the days of differentiation (Fig. 3 B). In addition, the large distributions of values in R2509C-Hom myocytes may be related to the variance of individual cellular functions involved in Ca^{2+} homeostasis. We found that $[Ca^{2+}]_{cyt}$ was elevated in R2509C-Hom myocytes at day 2 (176.6 ± 54.3 nM) after differentiation, as compared to those in WT (103.7 ± 40.7 nM) and R2509C-Het (124.5 ± 42.0 nM) myocytes ($P < 0.0001$ and 0.0001, respectively). Resting $[Ca^{2+}]_{cyt}$ increased with the days of differentiation, and the mean value was significantly high at day 4 of differentiation (222.5 ± 100.3 nM). To confirm the contribution of RYR1 mutants to the marked increase in $[Ca^{2+}]_{cyt}$, we tested the effects of Cpd1. Cpd1 (2 µM) was continuously applied to the culture media from the onset of differentiation. In R2509C-Hom myocytes, a significant decrease in resting $[Ca^{2+}]_{cyt}$ by Cpd1 was observed at day 3 (179.5 ± 63.2 and 140.6 ± 52.7 nM for myocytes in the absence and presence of Cpd1, respectively) and day 4 (222.5 ± 100.3 and 151.4 ± 73.5 nM for control and Cpd1, respectively; Fig. 3 B and Table 1). In addition, Western blot analysis of RYR1 was performed to examine the relationship between RYR1 expression level and increase in resting $[Ca^{2+}]_{cyt}$ in R2509C-Hom myocytes. As shown in Fig. 3 C, the expression

Table 1. **Resting $[Ca^{2+}]_{cyt}$ in WT and R2509C primary myocytes**

Genotype		$[Ca^{2+}]_{cyt}$ (nM)	n	N
WT	(d2-4)	103.7 ± 40.7	205	3
R2509C-Het	(d2-4)	124.5 ± 42.0	257	3
R2509C-Hom	(d2-4)	186.4 ± 71.4	776	4
R2509C-Hom	(d2)	176.6 ± 54.3	148	3
R2509C-Hom	(d3)	179.5 ± 63.2	494	4
R2509C-Hom	(d4)	222.5 ± 100.3	134	3
R2509C-Hom	2μM Cpd1 (d3)	140.6 ± 52.7	230	3
R2509C-Hom	2μM Cpd1 (d4)	151.4 ± 73.5	151	3

Values are mean ± SD.

level of RYR1 tended to increase depending on the differentiation days.

Excitation–contraction coupling and caffeine sensitivity

We next examined how excitation–contraction coupling is altered in mutant myocytes. Electrical stimulation induced significant Ca^{2+} transients (responses >10% of the baseline fluorescence value, i.e., F_0) in WT, R2509C-Het, and R2509C-Hom myocytes without apparent differences in the response rate (>90%). However, the peak amplitude of Ca^{2+} transients (F_{max}/F_0) was reduced in the order of WT ≥ R2509C-Het > R2509C-Hom (Fig. 4 A, Table 2), although the amplitude for R2509C-Hom may be somewhat underestimated due to an increase in F_0 in R2509C-Hom myocytes (see Fig. 3 A). Similarly, in KCl-induced depolarization, the peak amplitude of Ca^{2+} transients (F_{max}/F_0) at KCl concentrations above 20 mM was significantly reduced in the order of WT ≅ R2509C-Het > R2509C-Hom (Fig. 4 B and Table 2). To further characterize the functional properties of depolarization-induced Ca^{2+} transients, we plotted KCl dose-response curves. In each curve, the amplitude of Ca^{2+} transients was normalized by the maximum response to obtain the EC_{50} value (Fig. 4 C). The order of the sensitivity to KCl stimulation was R2509C-Hom > R2509C-Het > WT (Fig. 4 C and Table 2). Subsequently, we characterized caffeine-induced Ca^{2+} transients as an index for CICR activity (Fig. 4, D and E, and Table 2). Significant Ca^{2+} transients were observed at and above 3 mM in WT myocytes, whereas the corresponding caffeine concentrations for R2509C-Het and R2509C-Hom were 1 and 0.3 mM, respectively. As followed for the response to electrical stimulation, there were no significant differences between groups in the reaction rate (>90%) in the presence of 10 or 20 mM caffeine. Although the absolute peak amplitude (F_{max}/F_0) varied in the order of WT ≥ R2509C-Het > R2509C-Hom, the caffeine sensitivity was found to vary in the order of R2509C-Hom > R2509C-Het > WT (Fig. 4, D and E, and Table 2).

Heat-induced Ca^{2+} release in R2509C primary myocytes

We previously reported that Ca^{2+} transients are induced by infrared laser-based micro-heating in HEK293 cells expressing various RYR1 mutants as well as in isolated FDB fibers prepared from WT and R2509C-Het mice (Oyama et al., 2022). We found that mild heating (which did not affect $[Ca^{2+}]_{cyt}$ in WT muscle cells) significantly increased $[Ca^{2+}]_{cyt}$ in R2509C-Het muscle cells, demonstrating the heat-hypersensitivity of RYR1. Based on these results, we proposed a heat-mediated Ca^{2+} release mechanism through RYR1 from the SR, i.e., heat-induced Ca^{2+} release (HICR) that is likely to play a crucial role in the progression of MH at the cellular level (Oyama et al., 2022). Therefore, we next applied a heat pulse (ΔT = 11 ± 2°C from the base temperature T_0 = 24 ± 1°C; central value ± range) to primary myocytes from WT, R2509C-Het, and R2509C-Hom mice after loading with the fluorescent Ca^{2+} indicator Cal-520 (Fig. 5, A–F). An infrared laser beam focused with an objective lens formed a concentric temperature gradient around cells (Oyama et al., 2022). The temperature gradient obtained depends on the laser power used. In the present study, the maximum temperature rise was 13°C at the focal point, with a minimum of 10°C or less at the end of the field of view. The duration of heating was controlled by a mechanical shutter. The temperature gradient was formed within 0.1 s of the opening of the shutter, and then was eliminated within 0.1 s by heat diffusion when the shutter was closed (Itoh et al., 2014; Oyama et al., 2020). The change in temperature was calculated with temperature-sensitive fluorescent dextran (Oyama et al., 2015).

Then, we performed time-dependent analyses in WT, R2509C-Het, and R2509C-Hom myocytes. No significant differences were observed in Ca^{2+} level among the before (F_0), during (14–15 s), and after (19–20 s) heating in WT (Fig. 5 G). In R2509C-Het, $[Ca^{2+}]_{cyt}$ significantly increased during heating (Fig. 5 H), while in R2509C-Hom, it decreased during heating and increased after heating (Fig. 5 I). The fluorescence intensity of Cal-520 before heating was increased in the order of WT ≤ R2509C-Het < R2509C-Hom (Fig. 5 J), which is consistent with the order for the resting $[Ca^{2+}]_{cyt}$ (Fig. 3 A). Although little or no change in $[Ca^{2+}]_{cyt}$ was detected during heating in WT myocytes (Fig. 5, A and B; see thick black line), a substantial increase in $[Ca^{2+}]_{cyt}$ was detected in R2509C-Het myocytes (Fig. 5, C and D; see thick red line). The maximum changes in the relative fluorescence intensity of Cal-520 during heating ($\Delta F_{max}/F_0$) were greater in R2509C-Het myocytes than in WT or R2509C-Hom myocytes (Fig. 5 K and Fig. S4). This finding is consistent with our previous result obtained in isolated R2509C-Het FDB fibers (Oyama et al., 2022).

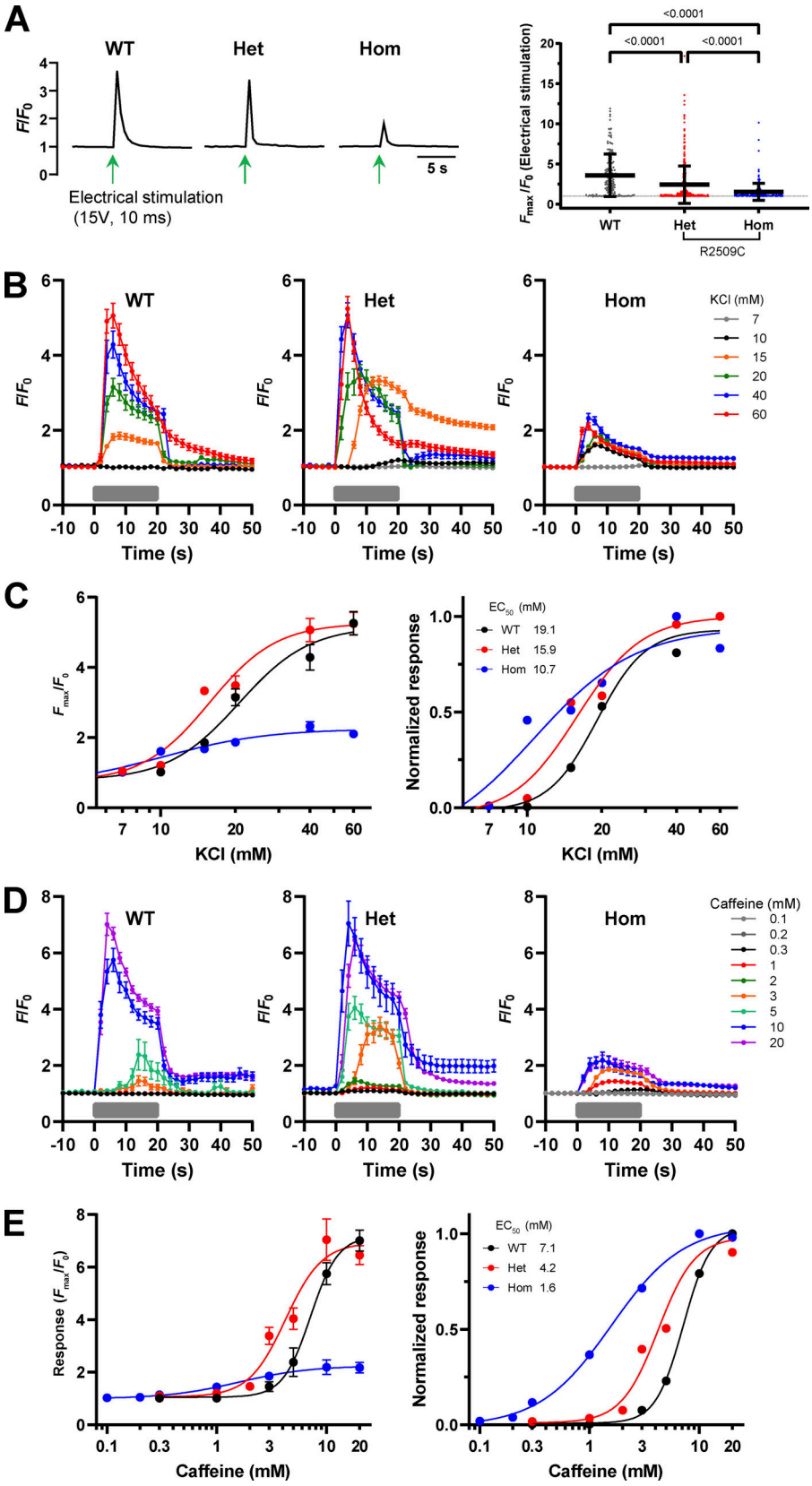

Figure 4. **Ca^{2+} transients by electrical stimulation or caffeine and KCl application in WT and R2509C-RYR1 primary myocytes. (A)** Left: Typical time course of Ca^{2+} transients induced by platinum field electrode stimulation (electrical stimulation; ES) in WT, R2509C-Het (Het), and R2509C-Hom (Hom) myocytes measured using Cal-520. The fluorescence intensity F was normalized to the initial value of F (F_0). Right: Graph showing peak amplitudes (F_{max}/F_0) of ES in WT (n = 176, N = 3), R2509C-Het (Het, n = 384, N = 4), and R2509C-Hom (Hom, n = 194, N = 3) primary myocytes. The horizontal dotted line indicates F_0. Values are mean ± SD. **(B)** K^+-induced depolarization in WT, R2509C-Het (Het) and R2509C-Hom (Hom) myocytes. KCl (7–60 mM) was applied at the time points indicated by the grey horizontal bar. Values are mean ± SEM (n = 36–107, N = 3, see Table 2). **(C)** Left: The magnitude of the peak Ca^{2+} transients was plotted against KCl concentrations and fitted to the dose–response curve in WT (black), R2509C-Het (red), and R2509C-Hom (blue). Right: Normalized for maximal peak amplitudes (F_{max}/F_0) to KCl. To eliminate run-down, only one dose was administered to the myocytes and the Ca^{2+} response was analyzed. **(D)** Ca^{2+} transients induced by caffeine in WT, R2509C-Het (Het), and R2509C-Hom (Hom) myocytes measured using Cal-520. Caffeine (0.1–20 mM) was applied at the time points indicated by the grey horizontal bar. Values are mean ± SEM (n = 20–104, N = 3, see Table 2). **(E)** Left: The magnitude of the peak Ca^{2+} transients was plotted against caffeine concentrations and fitted to the dose–response curve in WT (black), R2509C-Het (red), and R2509C-Hom (blue). Right: Normalized for maximal peak amplitudes (F_{max}/F_0) to caffeine. Curves are fittings based on the Hill equation: $R = Bottom + (Top - Bottom) \times C^{n'}/(C^{n'} + k^{n'})$, where R, C, k, and n' represent the normalized response, either KCl or caffeine concentration, EC_{50} and Hill coefficient. *Bottom* and *Top* represent the maximum and minimum responses. Statistical significance was determined using a one-way ANOVA with Tukey's test. Cells on days 2–4 after differentiation were analyzed. "n" indicates the number of myocytes, and "N" the number of animals.

Table 2. **Properties of Ca^{2+} transients by electrical stimulation, KCl, and caffeine**

	WT			R2509C-Het				R2509C-Hom			
	F_{max}/F_0	*n*	*N*	F_{max}/F_0	*n*	*N*	*p*	F_{max}/F_0	*n*	*N*	*p*
Electrical stimulation											
15V, 10 ms	3.59 ± 0.20	176	3	2.42 ± 0.12	384	4	<0.0001	1.53 ± 0.08	194	3	<0.0001
KCl (mM)											
7				1.05 ± 0.01	76	3		1.01 ± 0.01	94	3	
10	1.03 ± 0.01	76	3	1.21 ± 0.05	93	3	0.02	1.60 ± 0.05	107	3	<0.0001
15	1.85 ± 0.09	71	3	3.33 ± 0.11	92	3	<0.0001	1.67 ± 0.04	102	3	0.312
20	3.15 ± 0.24	71	3	3.48 ± 0.27	49	3	0.5139	1.86 ± 0.07	65	3	<0.0001
40	3.74 ± 0.29	51	3	5.07 ± 0.33	40	3	0.1746	2.32 ± 0.13	36	3	0.0003
60	5.06 ± 0.33	79	3	5.25 ± 0.33	65	3	0.9994	2.12 ± 0.10	62	3	<0.0001
EC_{50} (mM)	19.1			15.9				10.7			
Caffeine (mM)											
0.1								1.02 ± 0.01	52	3	
0.2								1.05 ± 0.01	47	3	
0.3	1.01 ± 0.01	28	3	1.10 ± 0.02	55	3	0.015	1.14 ± 0.03	28	3	<0.0001
1	1.01 ± 0.001	52	3	1.20 ± 0.04	101	3	0.0067	1.40 ± 0.04	104	3	<0.0001
2				1.46 ± 0.09	49	3					
3	1.46 ± 0.19	58	3	3.39 ± 0.33	55	3	0.0002	1.85 ± 0.07	87	3	0.285
5	2.38 ± 0.55	20	3	4.04 ± 0.41	38	3	0.0197				
10	5.80 ± 0.41	42	3	7.04 ± 0.80	61	3	0.3245	2.19 ± 0.28	35	3	<0.0001
20	7.01 ± 0.39	43	3	6.65 ± 0.36	70	3	0.7306	2.17 ± 0.20	73	3	<0.0001
EC_{50} (mM)	7.1			4.2				1.6			

Values are mean ± SEM. Statistical signification was determined by comparison with WT.

Why did R2509-Het cause a heat-induced Ca^{2+} release, whereas R2509C-Hom did not, and rather caused a decrease in $[Ca^{2+}]_{cyt}$? We recently reported that the ER/SR is a major Ca^{2+} source of the heat-induced Ca^{2+} bursts in HEK293 cells expressing WT and mutant RYR1 (Oyama et al., 2022), and that ER/SR Ca^{2+} is substantially depleted in cells expressing severe RYR1 mutation, such as R2509C. Subsequently, we tested whether the decrease in $[Ca^{2+}]_{cyt}$ during heating in R2509C-Hom myocytes is due to heat activation of SERCA. In R2509C-Hom myocytes, inhibition of SERCA by 20 µM CPA significantly suppressed the decrease in Ca^{2+} levels during heating (Fig. 6, A–D). The results suggest that ER/SR Ca^{2+} in R2509C-Hom myocytes were severely depleted, and heating caused Ca^{2+} uptake rather than Ca^{2+} release.

Simultaneous measurement of $[Ca^{2+}]_{cyt}$ and cellular temperature in isolated skeletal cells

Finally, we investigated whether an increase in the cellular temperature is associated with the increase in $[Ca^{2+}]_{cyt}$ upon application of anesthesia. In a previous study, we reported that inhalation of isoflurane increases the rectal temperature in R2509C-Het mice, and that the exposure to isoflurane increases the $[Ca^{2+}]_{cyt}$ in isolated FDB fibers (Yamazawa et al., 2021). At the cellular level, Meizoso-Huesca et al. (2022) demonstrated that heat production is closely related to Ca^{2+} leakage through RYR1 in the skeletal muscles, using a fluorescent molecular thermometer (Meizoso-Huesca et al., 2022). In the present study, we used ERthermAC, a small-molecule fluorescent dye (Kriszt et al., 2017), to perform the SR-targeted thermometry in living cells (Oyama et al., 2022). This dye is highly photostable and can be used with Cal-520 for intracellular Ca^{2+} imaging (e.g., Hou et al., 2017; Oyama et al., 2022). Striation patterns following ERthermAC treatment represent the morphology of the SR along myocytes, indicating successful staining by the dye (Fig. 7 A). We found that application of 1% isoflurane using a puffer pipette to R2509C-Het FDB fibers increased the fluorescence intensity of Cal-520 (Fig. 7 B, right top) and that of ERthermAC decreased (Fig. 7 B, right bottom). Note that the fluorescence intensity of ERthermAC decreased in response to an increase in temperature (as in Krisz et al., 2017; Hou et al., 2017; Oyama et al., 2022). WT FDB fibers showed no apparent decrease in the fluorescence intensity of Cal-520 or ERthermAC (Fig. 7 B, left), except for a gradual time-dependent reduction because of the photobleaching effect (Fig. S5). The results suggest that the prominent reduction in the fluorescence intensity of ERthermAC in R2509C-Het FDB fibers (Fig. 7 C) is not an artifact caused by application of isoflurane, but rather, at least partially, is due to the isoflurane-induced temperature increase in the cells.

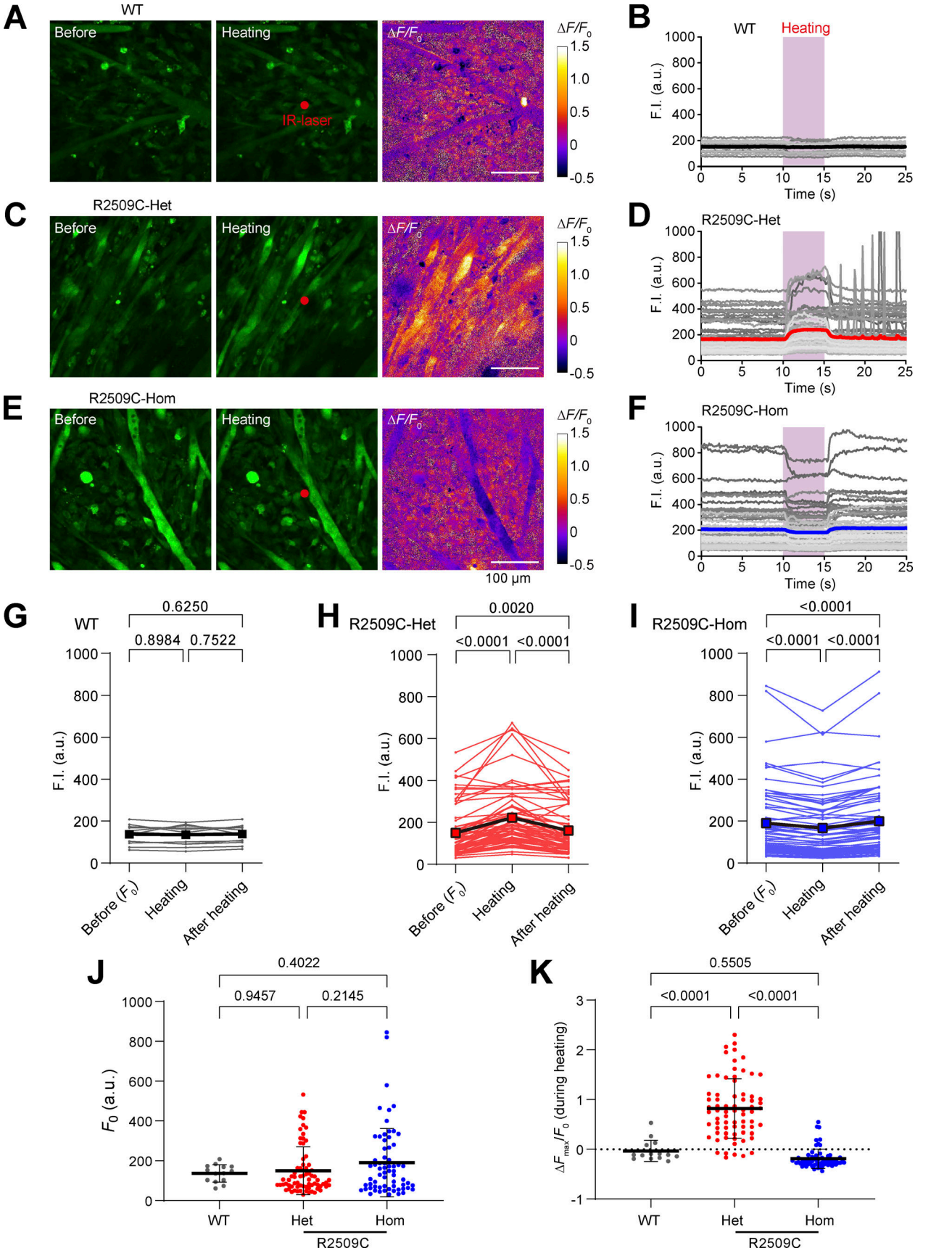

Figure 5. **Heat-induced Ca^{2+} release in WT and R2509C-RYR1 primary myocytes. (A)** Averaged fluorescence images of Cal-520–loaded WT myocytes before (left) and during heating (middle). Images captured for 1.2 s were averaged. Image on the right indicates the differences in fluorescence intensity

between the left and middle images ($\Delta F/F_0$). A closed red circle indicates the position of focused infrared (IR) laser beam for micro-heating. **(B)** Time-course of fluorescence intensity of Cal-520 in WT myocytes. Each line represents an individual primary myocyte. The pink vertical bar indicates the period of a heat pulse. **(C)** Same as in A for R2509C-Het myocytes. **(D)** Same as in B for R2509C-Het myocytes. **(E)** Same as in A for R2509C-Hom myocytes. **(F)** Same as in B for R2509C-Hom myocytes. **(G–I)** Time-dependent analyses in WT (G), R2509C-Het (H), and R2509C-Hom (I) myocytes. The Ca^{2+} levels before (F_0), during (14–15 s) and after (19–20 s) heating were analyzed. Thin lines represent individual cells, and thick line and squares represent averages. Data are analyzed by repeated measures one-way ANOVA with Tukey's multiple comparisons tests. **(J)** Basal fluorescence intensities of Cal-520 in WT, R2509C-Het, and R2509C-Hom myocytes before heating (F_0). **(K)** Maximum changes in the relative fluorescence intensity of Cal-520 during heating ($\Delta F_{max}/F_0$). Dotted horizontal line indicates the baseline. WT: n = 14, N = 3; R2509C-Het: n = 72, N = 4; R2509C-Hom: n = 66, N = 4. Myocytes from WT mice were analyzed 3 d after the onset of differentiation and those from R2509C-Het and R2509C-Hom 2–4 d after the onset of differentiation. Values are shown as mean ± SD. Statistical significance was determined using a one-way ANOVA with Tukey's test. ΔT = 11 ± 2°C; T_0 = 24 ± 1°C. "n" is the number of myocytes and "N" is the number of animals.

Discussion

We compared several aspects of Ca^{2+} dynamics (resting Ca^{2+}, KCl, caffeine) in primary cultured myocytes from recently generated MH model mice (R2509C mice). R2509C-Hom myocytes exhibited markedly increased resting $[Ca^{2+}]_{cyt}$, reduced depolarization evoked and caffeine-induced Ca^{2+} release, and lacked spontaneous Ca^{2+} transients. R2509C-Hom myocytes also exhibited significantly shortened sarcomeres, consistent with elevated resting $[Ca^{2+}]_{cyt}$. In addition, MH is induced by inhaled anesthetics to increase body temperature; however, the actual relationship between heat and Ca^{2+} transients remains unclear. Consequently, we measured $[Ca^{2+}]_{cyt}$ and cellular temperature simultaneously in the present study.

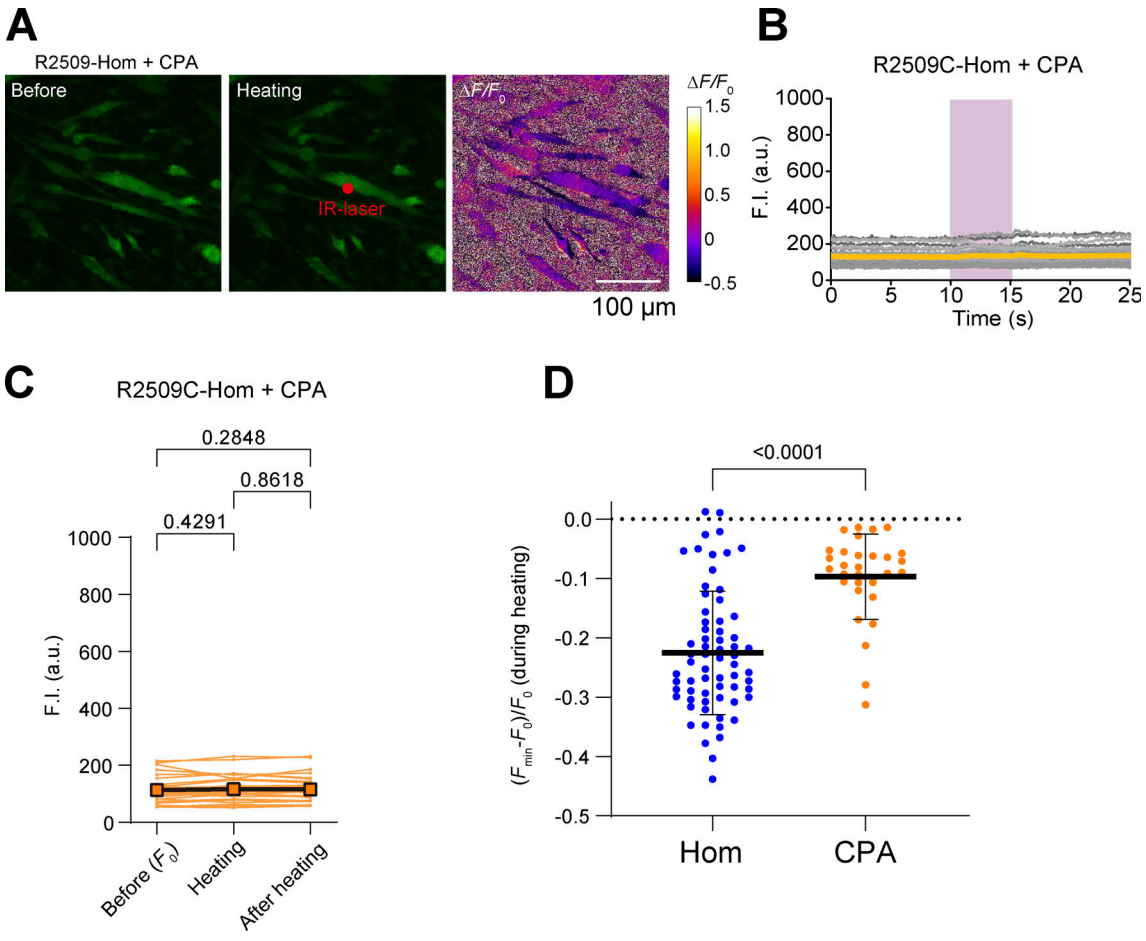

Figure 6. **Effect of cyclopiazonic acid on heat-induced Ca^{2+} release in R2509C-Hom primary myocytes. (A)** Averaged fluorescence images of Cal-520–loaded R2509C-Hom myocytes in the presence of 20 µM CPA before (left) and during heating (middle). Images captured for 1.2 s were averaged. The image on right indicates the differences in fluorescence intensity between left and middle images ($\Delta F/F_0$). A closed red circle indicates the position of focused infrared (IR) laser beam for micro-heating. **(B)** Time-course of fluorescence intensity of Cal-520 in R2509C-Hom + 20 µM CPA. Each line represents an individual primary myocyte. The pink vertical bar indicates the period of a heat pulse. ΔT = 11 ± 2°C; T_0 = 24 ± 1°C. **(C)** Time-dependent analyses of Cal-520 in R2509C-Hom + 20 µM CPA. The fluorescence intensity of Cal-520 before (0–1 s as F_0), during (14–15 s), and after (19–20 s) the heating in R2509C-Hom + 20 µM CPA. Thin lines represent individual cells. Thick line and squares represent averages. Data were analyzed by repeated measures one-way ANOVA with Tukey's multiple comparisons tests. **(D)** Minimum values in the relative fluorescence intensity of Cal-520 during heating [(F_{min} – F_0) / F_0]. Dotted horizontal line indicates the baseline. R2509C-Hom: n = 66, N = 4; R2509C-Hom + 20 µM CPA: n = 30, N = 3. Values are mean ± SD. Statistical significance was determined using a one-way ANOVA with Tukey's test. ΔT = 11 ± 2°C; T_0 = 24 ± 1°C. "n" is the number of myocytes and "N" is the number of animals.

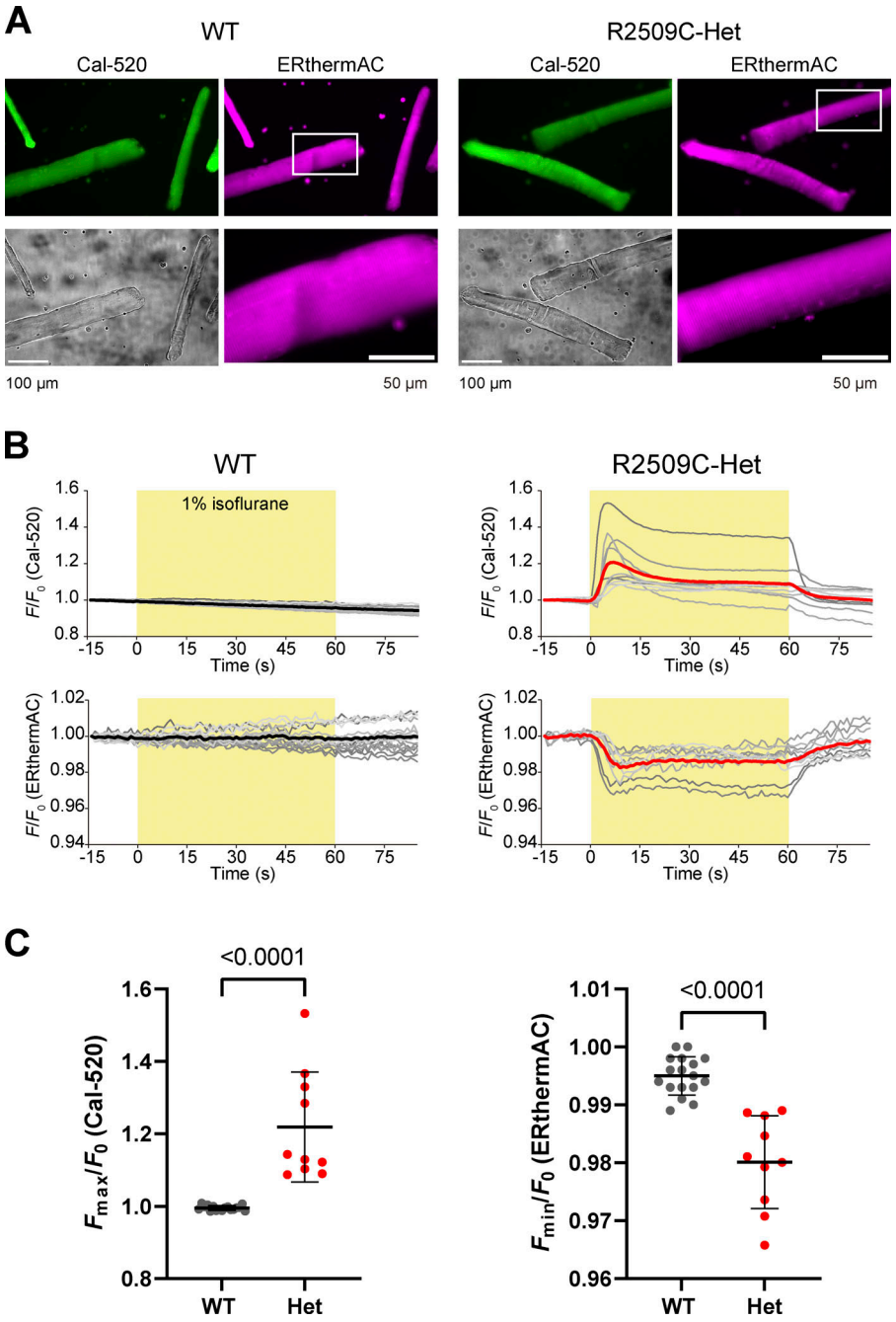

Figure 7. **Measurements of $[Ca^{2+}]_{cyt}$ and temperature of the sarcoplasmic reticulum in FDB fibers during isoflurane application. (A)** Bright-field (lower left panels) and fluorescence images of FDB fibers isolated from WT (left) and R2509C-Het (right) mice following co-staining with Cal-520 and ERthermAC. Lower right panels show higher magnification of the area depicted by white-outlined squares in upper right panels. **(B)** Time course of changes in the relative fluorescence intensity of Cal-520 (top) and ERthermAC (bottom) in WT (left) and R2509C-Het (right) cells. Gray lines represent individual cells. Thick colored lines represent average responses. Isoflurane (1%) was applied at the time points indicated by yellow horizontal bars. Photobleaching of ERthermAC was corrected by a single-exponential fitting (Arai et al., 2014). See Fig. S5 for raw data. **(C)** Maximum values (F_{max}/F_0) in the relative fluorescence intensity of Cal-520 (left) and minimum values (F_{min}/F_0) in the relative fluorescence intensity of ERthermAC (right) during isoflurane application. WT: n = 17, N = 4; R2509C-Het: n = 10, N = 4. Values are means ± SD. Statistical significance was determined using a one-way ANOVA with Tukey's test. "n" indicates the number of FDB fibers, and "N" the number of animals.

SL

There was no significant difference in the SL between WT and R2509C-Het myocytes, and the value was within the range reported for resting skeletal myocytes (i.e., 2.0–2.5 µm; Goldspink, 1968). In contrast, the SL of R2509C-Hom myocytes was abnormally shortened compared to those for WT or R2509C-Het myocytes. These findings are consistent with the notion that sarcomeres in R2509C-Hom myocytes are contracted even under resting conditions. Excessive shortening of SL has been reported around the core in the leg muscles of aged Y522S heterozygous mice (Boncompagni et al., 2009), which is consistent with our results.

We also analyzed the mechanisms by which SL was shortened to ∼1.7 µm in R2509C-Hom myocytes (Fig. 2). Samples for TEM imaging were chemically treated with glutaraldehyde, followed by dehydration (see Materials and methods). This protocol has been reported to reduce the size of cells by ∼10% (Wyffels, 2001). If this is the case, SL in living R2509C-Hom myocytes can be calculated within the ∼1.3–1.7 µm range, which is the physiologically relevant A-band length in vertebrate striated muscles (cf. Suzuki et al., 2005; Udaka et al., 2008; Shimomura et al., 2016). The short SL in R2509C-Hom myocytes indicates that abnormal contractions occur in these cells, even in the resting state. Such abnormal contractions can likely be induced by enhanced Ca^{2+} leakage from the SR, resulting in a sustained increase in $[Ca^{2+}]_{cyt}$ (Fig. 3 and Tables 1 and 2). Extensively elevated $[Ca^{2+}]_{cyt}$ may cause the disorganization of

myofibrillar structures in the skeletal muscles (Fig. S1), resulting in early death of R2509C-Hom embryos (see above).

The higher Ca^{2+} levels in R2509C-Het and R2509C-Hom myocytes than in WT (Fig. 3 A and Table 1) suggest that SL is equal to that in WT, or shortened due to tension generation according to the pCa-tension curve. R2509C-Het was well fit by a Gaussian, showing the peak and the SD as 2.3 µm (Fig. 2 D), which is quite similar to the case in WT, and their distributions are not significantly different (Fig. 2 C). Therefore, we can conclude that Ca^{2+} level distribution in R2509C-Het myocytes was in the region of relaxation. However, R2509C-Hom and R2509C-Hom+Cpd1 were not fit well by a single Gaussian. Therefore, we switch to the other possibility that the distribution of Ca^{2+} level is centered at the overlapping region between the relaxed and the partially activated state; hence, there are two respective distributions. These findings are consistent with those of previous studies (Balnave and Allen, 1996; Glass et al., 2018); i.e., in mouse FDB fibers, active force through actomyosin interaction is generated from 150 nM $[Ca^{2+}]_{cyt}$, and $[Ca^{2+}]_{cyt}$ for half-maximal activation is 314 nM (Balnave and Allen, 1996; Glass et al., 2018). The SL of a myocyte in the group in the relaxed state should be similar to that in the WT that is also in the relaxed state. Therefore, the distributions of R2509C-Hom and R2509C-Hom+Cpd1 were analyzed based on two Gaussians, where one of the peaks was fixed at 2.2 µm. According to this analysis, the shorter peak is at 1.6 µm in R2509C-Hom, and it is recovered slightly to 1.8 µm in R2509C-Hom+Cpd1 (Fig. 2 D).The remarkable differences in the SL distributions of R2509C-Het and R2509C-Hom are consistent with the less significant difference of the resting $[Ca^{2+}]_{cyt}$ between WT and R2509C-Het myocytes when compared with that between R2509C-Het and R2509C-Hom (Fig. 3 A). It is also noticeable that the population at 2.2 µm that corresponds to the sarcomere in the relaxed state is higher in R2509C-Hom+Cpd1 than in R2509C-Hom. The recovery of SL to the longer distributions strongly suggests that the Ca^{2+} level, and in turn the tension level, was lowered in the presence of Cpd1.

$[Ca^{2+}]_{cyt}$ homeostasis

It has been reported that the expression of RYR1 mRNA, which is not expressed in pre-differentiated myoblasts, is induced at ∼24 h after the onset of differentiation, with the expression level reaching the maximum at day 4 (Aley et al., 2010). Given this previous finding, the abrupt increase in the resting $[Ca^{2+}]_{cyt}$ in R2509C-Hom myocytes at day 4 is likely coupled with an increase in RYR1 expression and Ca^{2+} leakage from the SR. This prediction is supported by our previous result on R2508C RYR1-mediated Ca^{2+} leakage from the ER in HEK293 cells expressing mutant RYR1 (Murayama et al., 2016). This indicated that the increase in resting $[Ca^{2+}]_{cyt}$ in R2509C-Het and R2509C-Hom myocytes is caused by enhanced Ca^{2+} leakage through RYR1 from the SR.

Notably, F_{max}/F_0 in R2509C-Hom myocytes were unexpectedly low relative to those in WT or R2509C-Het myocytes, although it is underestimated because F_0 is increased. The results suggest that Ca^{2+} concentration in the SR lumen of R2509C-Hom myocytes was markedly reduced, as observed in the ER lumen with HEK293 cells overexpressing R2508C mutants (Murayama et al., 2016). In addition, the F_{max}/F_0 induced by 10 or 20 mM caffeine reportedly represents the maximal response of Ca^{2+} released from the SR/ER (Murayama et al., 2015; Murayama et al., 2016; Yamazawa et al., 2020). Therefore, we calculated the F_{max}/F_0 values under electrical stimulation and under maximal caffeine. As summarized in Table 2, the ratio values of WT (0.51: 3.59/7.01) and R2509C-Het (0.34: 2.42/7.04) myocytes were comparable, whereas the ratio values (0.70: 1.53/2.19) in R2509C-Hom myocytes were markedly greater than the others; therefore, the sensitivity to depolarization was likely increased in these cells. The increased sensitivity to depolarization in R2509C-Hom myocytes was also indicated by the EC_{50} values determined from the dose–response curve for KCl (Fig. 4, B and C; and Table 2). These findings are consistent with those of a previous study showing increased sensitivity to K^+-induced depolarization in myotubes from homozygous R163C mice (Yang et al., 2006).

Heat-induced Ca^{2+} release and cell temperature

In R2509C-Hom myocytes, fluorescence intensity was lower during heating and higher after heating than before heating (Fig. 5, E and F; and Fig. S4), coupled presumably with the heat-induced Ca^{2+} release mechanism, as demonstrated in our previous study using R2508C HEK293 cells (Oyama et al., 2022). CPA, a SERCA inhibitor, inhibited the decrease in $[Ca^{2+}]_{cyt}$ during heating in R2509C-Hom myocytes (Fig. 6 D). This result may have been caused by thermal activation of the SERCA, as demonstrated in our previous studies (Tseeb et al., 2009; Itoh et al., 2014; Oyama et al., 2022). This is because $[Ca^{2+}]_{cyt}$ is increased in R2509C-Hom myocytes coupled with decreased $[Ca^{2+}]$ in the SR lumen; therefore, $[Ca^{2+}]_{cyt}$ is lowered via heating-induced activation of SERCA. Hence, the differential Ca^{2+} response in R2509C-Het versus R2509C-Hom myocytes may be attributable to a difference in Ca^{2+} concentration between the cytoplasm and SR lumen.

The fluorescence intensity of ERthermAC started to decrease with a delay after onset of the isoflurane-induced Ca^{2+} increase (Fig. 7 B). A similar type of delay was observed in our previous studies using HeLa cells (Suzuki et al., 2007; Takei et al., 2014). The delay of a temperature increase following an increase in $[Ca^{2+}]_{cyt}$ may reflect the time for SERCA to be activated for its thermogenesis, as efficient heat release by the Ca^{2+}-ATPase should occur only after $[Ca^{2+}]_{SR}$ is lowered to a certain value (de Meis et al., 2005). In the present study, this hypothesis was directly tested in R2509C-Hom myocytes, in which Ca^{2+} concentration in the SR was significantly reduced compared to that in WT and R2509C-Het myocytes (Fig. 3 and Table 1). We consider that in R2509C-Hom myocytes, the thermogenic activity of SERCA is immediately increased after onset of the isoflurane-induced Ca^{2+} increase and, therefore, the temperature increases with a shorter delay.

However, this experimentation could not be performed in primary myocytes because of the pre-differentiated myoblasts (MF20-negative cells) present at high density, which caused a strong background signal overlapping that of primary myocytes (Fig. 1 B and Fig. S6). Further studies are required to resolve this

technical issue by developing (1) a method of obtaining differentiated myoblasts from primary myocytes with a sufficiently homogeneous quality and (2) a fluorescent probe that specifically targets the SR in living skeletal muscles.

In summary, we analyzed morphological and functional changes in myocytes from R2509C-RYR1 mice. In R2509C-Hom myocytes, Ca^{2+} release by depolarization or caffeine was decreased and resting $[Ca^{2+}]_{cyt}$ was increased, indicating a Ca^{2+} leak and a reduced SR Ca^{2+} content. In R2509C-Hom myocytes, sarcomeres were remarkably shortened to the A-band length, even in the resting condition, which was associated with abnormal Ca^{2+} homeostasis, particularly an increase in the resting $[Ca^{2+}]_{cyt}$. In R2509C-Het myocytes, heat sensitivity for intracellular Ca^{2+} release via the heat-induced Ca^{2+} release mechanism was increased, and the cellular temperature was elevated in the presence of isoflurane. These findings suggest that (1) the abnormal morphological and functional changes underlie the embryonic lethality of homozygotes, and (2) environmental heat stress or exposure to an inhalation anesthetic, or both, accelerates the progression of MH in heterozygotes.

Acknowledgments

Eduardo Ríos served as editor.

We would like to thank Dr. Togo Shimozawa (The University of Tokyo) for critical reading of the manuscript, and Ms. Ikue Hiraga (Juntendo University) for her technical assistance. We thank Dr. Young-Tae Chang (Pohang University of Science and Technology, Gyeongsangbuk, Korea) for provision of ERthermAC.

This work was supported by JSPS KAKENHI Grant Numbers 19K07306, 20H04511, 21K09755 22H05055 (to T. Yamazawa), 22H05053 (to M. Suzuki), 22H05054 (to K. Oyama), 21K06789 (to F. Kobirumaki-Shimozawa), 20H03421, 21K19929 (to N. Fukuda), 19H03404, 22H02805 (to T. Murayama), 19K07105 (to N. Kurebayashi), 19H03198 (to K. Oyama, T. Yamazawa, and M. Suzuki), and 22H03198 (to N. Fukuda, F. Kobirumaki-Shimozawa, and T. Yamazawa), and the Platform Project for Supporting Drug Discovery and Life Science Research (BINDS; Basis for Supporting Innovative Drug Discovery and Life Science Research) from AMED under Grant Number JP20am0101080 (to T. Murayama and N. Kurebayashi, support No. 2533), Vehicle Racing Commemorative Foundation (#6237, 6303 to T. Murayama), and The Naito Foundation (to F. Kobirumaki-Shimozawa), and an Intramural Research Grant for Neurological and Psychiatric Disorders from the National Center of Neurology and Psychiatry (2-5 to T. Murayama).

The authors declare no competing financial interests.

Author contributions: T. Yamazawa, K. Oyama, N. Fukuda, and M. Suzuki designed the research study; Y. Tsuboi, T. Yamazawa, F. Kobirumaki-Shimozawa, T. Murayama, N. Kurebayashi, Y. Manome, E. Kikuchi, and T. Tachibana performed the experiments; S. Noguchi, T. Inoue, Y.U. Inoue, S. Mori, R. Ishida, H. Kagechika, and I. Nishino contributed new reagents/analytic tools; Y. Tsuboi, K. Oyama, M. Suzuki, N. Fukuda, and T. Yamazawa analyzed the data. All authors were involved in drafting this work.

Submitted: 24 February 2022
Revised: 22 July 2022
Accepted: 14 September 2022

References

Aley, P.K., A.M. Mikolajczyk, B. Munz, G.C. Churchill, A. Galione, and F. Berger. 2010. Nicotinic acid adenine dinucleotide phosphate regulates skeletal muscle differentiation via action at two-pore channels. *Proc. Natl. Acad. Sci. USA*. 107:19927–19932. https://doi.org/10.1073/pnas.1007381107

Allard, B. 2018. From excitation to intracellular Ca^{2+} movements in skeletal muscle: Basic aspects and related clinical disorders. *Neuromuscul. Disord.* 28:394–401. https://doi.org/10.1016/j.nmd.2018.03.004

Arai, S., S.-C. Lee, D. Zhai, M. Suzuki, and Y.T. Chang. 2014. A molecular fluorescent probe for targeted visualization of temperature at the endoplasmic reticulum. *Sci. Rep.* 4:6701. https://doi.org/10.1038/srep06701

Balnave, C.D., and D.G. Allen. 1996. The effect of muscle length on intracellular calcium and force in single fibres from mouse skeletal muscle. *J. Physiol.* 492 (Pt 3):705–713. https://doi.org/10.1113/jphysiol.1996.sp021339

Boncompagni, S., A.E. Rossi, M. Micaroni, S.L. Hamilton, R.T. Dirksen, C. Franzini-Armstrong, and F. Protasi. 2009. Characterization and temporal development of cores in a mouse model of malignant hyperthermia. *Proc. Natl. Acad. Sci. USA*. 106:21996–22001. https://doi.org/10.1073/pnas.0911496106

Chelu, M.G., S.A. Goonasekera, W.J. Durham, W. Tang, J.D. Lueck, J. Riehl, I.N. Pessah, P. Zhang, M.B. Bhattacharjee, R.T. Dirksen, and S.L. Hamilton. 2006. Heat- and anesthesia-induced malignant hyperthermia in an RyR1 knock-in mouse. *FASEB J.* 20:329–330. https://doi.org/10.1096/fj.05-4497fje

Davis, M., R. Brown, A. Dickson, H. Horton, D. James, N. Laing, R. Marston, M. Norgate, D. Perlman, N. Pollock, and K. Stowell. 2002. Malignant hyperthermia associated with exercise-induced rhabdomyolysis or congenital abnormalities and a novel RYR1 mutation in New Zealand and Australian pedigrees. *Br. J. Anaesth.* 88:508–515. https://doi.org/10.1093/bja/88.4.508

des Georges, A., O.B. Clarke, R. Zalk, Q. Yuan, K.J. Condon, R.A. Grassucci, W.A. Hendrickson, A.R. Marks, and J. Frank. 2016. Structural Basis for gating and activation of RyR1. *Cell*. 167:145–157.e17. https://doi.org/10.1016/j.cell.2016.08.075

de Meis, L., A.P. Arruda, and D.P. Carvalho. 2005. Role of sarco/endoplasmic reticulum Ca^{2+}-ATPase in thermogenesis. *Biosci. Rep.* 25:181–190. https://doi.org/10.1007/s10540-005-2884-7

Efremov, R.G., A. Leitner, R. Aebersold, and S. Raunser. 2015. Architecture and conformational switch mechanism of the ryanodine receptor. *Nature*. 517:39–43. https://doi.org/10.1038/nature13916

Endo, M. 2009. Calcium-induced calcium release in skeletal muscle. *Physiol. Rev.* 89:1153–1176. https://doi.org/10.1152/physrev.00040.2008

Glass, L.D., A.J. Cheng, and B.R. MacIntosh. 2018. Role of Ca^{2+} in changing active force during intermittent submaximal stimulation in intact, single mouse muscle fibers. *Pflugers Arch.* 470:1243–1254. https://doi.org/10.1007/s00424-018-2143-y

Goldspink, G. 1968. Sarcomere length during post-natal growth of mammalian muscle fibres. *J. Cell Sci.* 3:539–548. https://doi.org/10.1242/jcs.3.4.539

Grynkiewicz, G., M. Poenie, and R.Y. Tsien. 1985. A new generation of Ca^{2+} indicators with greatly improved fluorescence properties. *J. Biol. Chem.* 260:3440–3450. https://doi.org/10.1016/s0021-9258(19)83641-4

Harkins, A.B., N. Kurebayashi, and S.M. Baylor. 1993. Resting myoplasmic free calcium in frog skeletal muscle fibers estimated with fluo-3. *Biophys. J.* 65:865–881. https://doi.org/10.1016/S0006-3495(93)81112-3

Hou, Y., T. Kitaguchi, R. Kriszt, Y.H. Tseng, M. Raghunath, and M. Suzuki. 2017. Ca^{2+}associated triphasic pH changes in mitochondria during brown adipocyte activation. *Mol. Metabol.* 6:797–808. https://doi.org/10.1016/j.molmet.2017.05.013

Iino, M. 1999. Molecular aspects of the excitation-contraction coupling in skeletal muscle. *Jpn. J. Physiol.* 49:325–333. https://doi.org/10.2170/jjphysiol.49.325

Itoh, H., K. Oyama, M. Suzuki, and S. Ishiwata. 2014. Microscopic heat pulse-induced calcium dynamics in single WI-38 fibroblasts. *Biophysics*. 10:109–119. https://doi.org/10.2142/biophysics.10.109

Jungbluth, H., S. Treves, F. Zorzato, A. Sarkozy, J. Ochala, C. Sewry, R. Phadke, M. Gautel, and F. Muntoni. 2018. Congenital myopathies: Disorders of excitation-contraction coupling and muscle contraction. *Nat. Rev. Neurol.* 14:151–167. https://doi.org/10.1038/nrneurol.2017.191

Konishi, M., A. Olson, S. Hollingworth, and S.M. Baylor. 1988. Myoplasmic binding of fura-2 investigated by steady-state fluorescence and absorbance measurements. *Biophys. J.* 54:1089–1104. https://doi.org/10.1016/S0006-3495(88)83045-5

Kriszt, R., S. Arai, H. Itoh, M.H. Lee, A.G. Goralczyk, X.M. Ang, A.M. Cypess, A.P. White, F. Shamsi, R. Xue, et al. 2017. Optical visualisation of thermogenesis in stimulated single-cell brown adipocytes. *Sci. Rep.* 7: 1383. https://doi.org/10.1038/s41598-017-00291-9

Lanner, J.T., D.K. Georgiou, A.D. Joshi, and S.L. Hamilton. 2010. Ryanodine receptors: Structure, expression, molecular details, and function in calcium release. *Cold Spring Harbor Perspect. Biol.* 2:a003996. https://doi.org/10.1101/cshperspect.a003996

Lopez, J.R., V. Kaura, C.P. Diggle, P.M. Hopkins, and P.D. Allen. 2018. Malignant hyperthermia, environmental heat stress, and intracellular calcium dysregulation in a mouse model expressing the p.G2435R variant of RYR1. *Br. J. Anaesth.* 121:953–961. https://doi.org/10.1016/j.bja.2018.07.008

Meissner, G. 1994. Ryanodine receptor/Ca^{2+} release channels and their regulation by endogenous effectors. *Annu. Rev. Physiol.* 56:485–508. https://doi.org/10.1146/annurev.ph.56.030194.002413

Meizoso-Huesca, A., L. Pearce, C.J. Barclay, and B.S. Launikonis. 2022. Ca^{2+} leak through ryanodine receptor 1 regulates thermogenesis in resting skeletal muscle. *Proc. Natl. Acad. Sci. USA.* 119:e2119203119. https://doi.org/10.1073/pnas.2119203119

Mori, S., H. Iinuma, N. Manaka, M. Ishigami-Yuasa, T. Murayama, Y. Nishijima, A. Sakurai, R. Arai, N. Kurebayashi, T. Sakurai, and H. Kagechika. 2019. Structural development of a type-1 ryanodine receptor (RyR1) Ca^{2+}-release channel inhibitor guided by endoplasmic reticulum Ca^{2+} assay. *Eur. J. Med. Chem.* 179:837–848. https://doi.org/10.1016/j.ejmech.2019.06.076

Murayama, T., N. Kurebayashi, T. Yamazawa, H. Oyamada, J. Suzuki, K. Kanemaru, K. Oguchi, M. Iino, and T. Sakurai. 2015. Divergent activity profiles of type 1 ryanodine receptor channels carrying malignant hyperthermia and central core disease mutations in the amino-terminal region. *PLoS One.* 10:e0130606. https://doi.org/10.1371/journal.pone.0130606

Murayama, T., N. Kurebayashi, H. Ogawa, T. Yamazawa, H. Oyamada, J. Suzuki, K. Kanemaru, K. Oguchi, M. Iino, and T. Sakurai. 2016. Genotype-phenotype correlations of malignant hyperthermia and central core disease mutations in the central region of the RYR1 channel. *Hum. Mutat.* 37:1231–1241. https://doi.org/10.1002/humu.23072

Oyama, K., T. Arai, A. Isaka, T. Sekiguchi, H. Itoh, Y. Seto, M. Miyazaki, T. Itabashi, T. Ohki, M. Suzuki, and S. Ishiwata. 2015. Directional bleb formation in spherical cells under temperature gradient. *Biophys. J.* 109: 355–364. https://doi.org/10.1016/j.bpj.2015.06.016

Oyama, K., M. Gotoh, Y. Hosaka, T.G. Oyama, A. Kubonoya, Y. Suzuki, T. Arai, S. Tsukamoto, Y. Kawamura, H. Itoh, et al. 2020. Single-cell temperature mapping with fluorescent thermometer nanosheets. *J. Gen. Physiol.* 152:e201912469. https://doi.org/10.1085/jgp.201912469

Oyama, K., V. Zeeb, T. Yamazawa, N. Kurebayashi, F. Kobirumaki-Shimozawa, T. Murayama, H. Oyamada, S. Noguchi, T. Inoue, Y.U. Inoue, et al. 2022. Heat-hypersensitive mutants of ryanodine receptor type 1 revealed by microscopic heating. *Proc. Natl. Acad. Sci. USA.* 119: e2201286119. https://doi.org/10.1073/pnas.2201286119

Pancaroglu, R., and F. Van Petegem. 2018. Calcium channelopathies: Structural insights into disorders of the muscle excitation-contraction complex. *Annu. Rev. Genet.* 52:373–396. https://doi.org/10.1146/annurev-genet-120417-031311

Rando, T.A., and H.M. Blau. 1994. Primary mouse myoblast purification, characterization, and transplantation for cell-mediated gene therapy. *J. Cell Biol.* 125:1275–1287. https://doi.org/10.1083/jcb.125.6.1275

Rios, E. 2018. Calcium-induced release of calcium in muscle: 50 years of work and the emerging consensus. *J. Gen. Physiol.* 150:521–537. https://doi.org/10.1085/jgp.201711959

Royer, L., S. Pouvreau, and E. Rios. 2008. Evolution and modulation of intracellular calcium release during long-lasting, depleting depolarization in mouse muscle. *J. Physiol.* 586:4609–4629. https://doi.org/10.1113/jphysiol.2008.157990

Schneider, M.F. 1994. Control of calcium release in functioning skeletal muscle fibers. *Annu. Rev. Physiol.* 56:463–484. https://doi.org/10.1146/annurev.ph.56.030194.002335

Shimomura, T., H. Iwamoto, T.T. Vo Doan, S. Ishiwata, H. Sato, and M. Suzuki. 2016. A beetle flight muscle displays leg muscle microstructure. *Biophys. J.* 111:1295–1303. https://doi.org/10.1016/j.bpj.2016.08.013

Sinha, A.K., P. Kumari, M.M. Vaghela, C. Sinha, and B. Kumar. 2017. Postoperative malignant hyperthermia- A medical emergency: A case report and review of literature. *J. Clin. Diagn. Res.* 11:PD01–PD02. https://doi.org/10.7860/JCDR/2017/20531.9493

Suzuki, M., H. Fujita, and S. Ishiwata. 2005. A new muscle contractile system composed of a thick filament lattice and a single actin filament. *Biophys. J.* 89:321–328. https://doi.org/10.1529/biophysj.104.054957

Suzuki, M., V. Tseeb, K. Oyama, and S. Ishiwata. 2007. Microscopic detection of thermogenesis in a single HeLa cell. *Biophys. J.* 92:L46–L48. https://doi.org/10.1529/biophysj.106.098673

Takei, Y., S. Arai, A. Murata, M. Takabayashi, K. Oyama, S. Ishiwata, S. Takeoka, and M. Suzuki. 2014. A nanoparticle-based ratiometric and self-calibrated fluorescent thermometer for single living cells. *ACS Nano.* 8:198–206. https://doi.org/10.1021/nn405456e

Takeshima, H., M. Iino, H. Takekura, M. Nishi, J. Kuno, O. Minowa, H. Takano, and T. Noda. 1994. Excitation-contraction uncoupling and muscular degeneration in mice lacking functional skeletal muscle ryanodine-receptor gene. *Nature.* 369:556–559. https://doi.org/10.1038/369556a0

Tong, J., H. Oyamada, N. Demaurex, S. Grinstein, T.V. McCarthy, and D.H. MacLennan. 1997. Caffeine and halothane sensitivity of intracellular Ca^{2+} release is altered by 15 calcium release channel (ryanodine receptor) mutations associated with malignant hyperthermia and/or central core disease. *J. Biol. Chem.* 272:26332–26339. https://doi.org/10.1074/jbc.272.42.26332

Tong, J., T.V. McCarthy, and D.H. MacLennan. 1999. Measurement of resting cytosolic Ca^{2+} concentrations and Ca^{2+} store size in HEK-293 cells transfected with malignant hyperthermia or central core disease mutant Ca^{2+} release channels. *J. Biol. Chem.* 274:693–702. https://doi.org/10.1074/jbc.274.2.693

Treves, S., H. Jungbluth, F. Muntoni, and F. Zorzato. 2008. Congenital muscle disorders with cores: The ryanodine receptor calcium channel paradigm. *Curr. Opin. Pharmacol.* 8:319–326. https://doi.org/10.1016/j.coph.2008.01.005

Tseeb, V., M. Suzuki, K. Oyama, K. Iwai, and S. Ishiwata. 2009. Highly thermosensitive Ca^{2+} dynamics in a HeLa cell through IP3 receptors. *HFSP J.* 3:117–123. https://doi.org/10.2976/1.3073779

Tung, C.C., P.A. Lobo, L. Kimlicka, and F. Van Petegem. 2010. The amino-terminal disease hotspot of ryanodine receptors forms a cytoplasmic vestibule. *Nature.* 468:585–588. https://doi.org/10.1038/nature09471

Udaka, J., S. Ohmori, T. Terui, I. Ohtsuki, S. Ishiwata, S. Kurihara, and N. Fukuda. 2008. Disuse-induced preferential loss of the giant protein titin depresses muscle performance via abnormal sarcomeric organization. *J. Gen. Physiol.* 131:33–41. https://doi.org/10.1085/jgp.200709888

Uto, A., H. Arai, and Y. Ogawa. 1991. Reassessment of Fura-2 and the ratio method for determination of intracellular Ca^{2+} concentrations. *Cell Calcium.* 12:29–37. https://doi.org/10.1016/0143-4160(91)90082-p

Wappler, F., M. Fiege, M. Steinfath, K. Agarwal, J. Scholz, S. Singh, J. Matschke, and J. Schulte Am Esch. 2001. Evidence for susceptibility to malignant hyperthermia in patients with exercise-induced rhabdomyolysis. *Anesthesiology.* 94:95–100. https://doi.org/10.1097/00000542-200101000-00019

Woll, K.A., and F. Van Petegem. 2022. Calcium-release channels: Structure and function of IP_3 receptors and ryanodine receptors. *Physiol. Rev.* 102: 209–268. https://doi.org/10.1152/physrev.00033.2020

Wyffels, J.T. 2001. Principles and Techniques of Electron Microscopy: Biological Applications, Fourth Edition, by M.A.Hayat. Microsc. Microanal. 7:66

Yamazawa, T., H. Takeshima, T. Sakurai, M. Endo, and M. Iino. 1996. Subtype specificity of the ryanodine receptor for Ca^{2+} signal amplification in excitation-contraction coupling. *EMBO J.* 15:6172–6177. https://doi.org/10.1002/j.1460-2075.1996.tb01005.x

Yamazawa, T., H. Takeshima, M. Shimuta, and M. Iino. 1997. A region of the ryanodine receptor critical for excitation-contraction coupling in skeletal muscle. *J. Biol. Chem.* 272:8161–8164. https://doi.org/10.1074/jbc.272.13.8161

Yamazawa, T., N. Nakamura, M. Sato, and C. Sato. 2016. Secretory glands and microvascular systems imaged in aqueous solution by atmospheric scanning electron microscopy (ASEM). *Microsc. Res. Tech.* 79:1179–1187. https://doi.org/10.1002/jemt.22773

Yamazawa, T., H. Ogawa, T. Murayama, M. Yamaguchi, H. Oyamada, J. Suzuki, N. Kurebayashi, K. Kanemaru, K. Oguchi, T. Sakurai, and M. Iino.

2020. Insights into channel modulation mechanism of RYR1 mutants using Ca^{2+} imaging and molecular dynamics. *J. Gen. Physiol.* 152: e201812235. https://doi.org/10.1085/jgp.201812235

Yamazawa, T., T. Kobayashi, N. Kurebayashi, M. Konishi, S. Noguchi, T. Inoue, Y.U. Inoue, I. Nishino, S. Mori, H. Iinuma, et al. 2021. A novel RyR1-selective inhibitor prevents and rescues sudden death in mouse models of malignant hyperthermia and heat stroke. *Nat. Commun.* 12: 4293. https://doi.org/10.1038/s41467-021-24644-1

Yan, Z., X. Bai, C. Yan, J. Wu, Z. Li, T. Xie, W. Peng, C. Yin, X. Li, S.H.W. Scheres, et al. 2015. Structure of the rabbit ryanodine receptor RyR1 at near-atomic resolution. *Nature*. 517:50–55. https://doi.org/10.1038/nature14063

Yang, T., J. Riehl, E. Esteve, K.I. Matthaei, S. Goth, P.D. Allen, I.N. Pessah, and J.R. Lopez. 2006. Pharmacologic and functional characterization of malignant hyperthermia in the R163C RyR1 knock-in mouse. *Anesthesiology*. 105:1164–1175. https://doi.org/10.1097/00000542-200612000-00016

Yuen, B., S. Boncompagni, W. Feng, T. Yang, J.R. Lopez, K.I. Matthaei, S.R. Goth, F. Protasi, C. Franzini-Armstrong, P.D. Allen, and I.N. Pessah. 2012. Mice expressing T4826I-RYR1 are viable but exhibit sex- and genotype-dependent susceptibility to malignant hyperthermia and muscle damage. *FASEB J.* 26:1311–1322. https://doi.org/10.1096/fj.11-197582

Zalk, R., O.B. Clarke, A. des Georges, R.A. Grassucci, S. Reiken, F. Mancia, W.A. Hendrickson, J. Frank, and A.R. Marks. 2015. Structure of a mammalian ryanodine receptor. *Nature*. 517:44–49. https://doi.org/10.1038/nature13950

Supplemental material

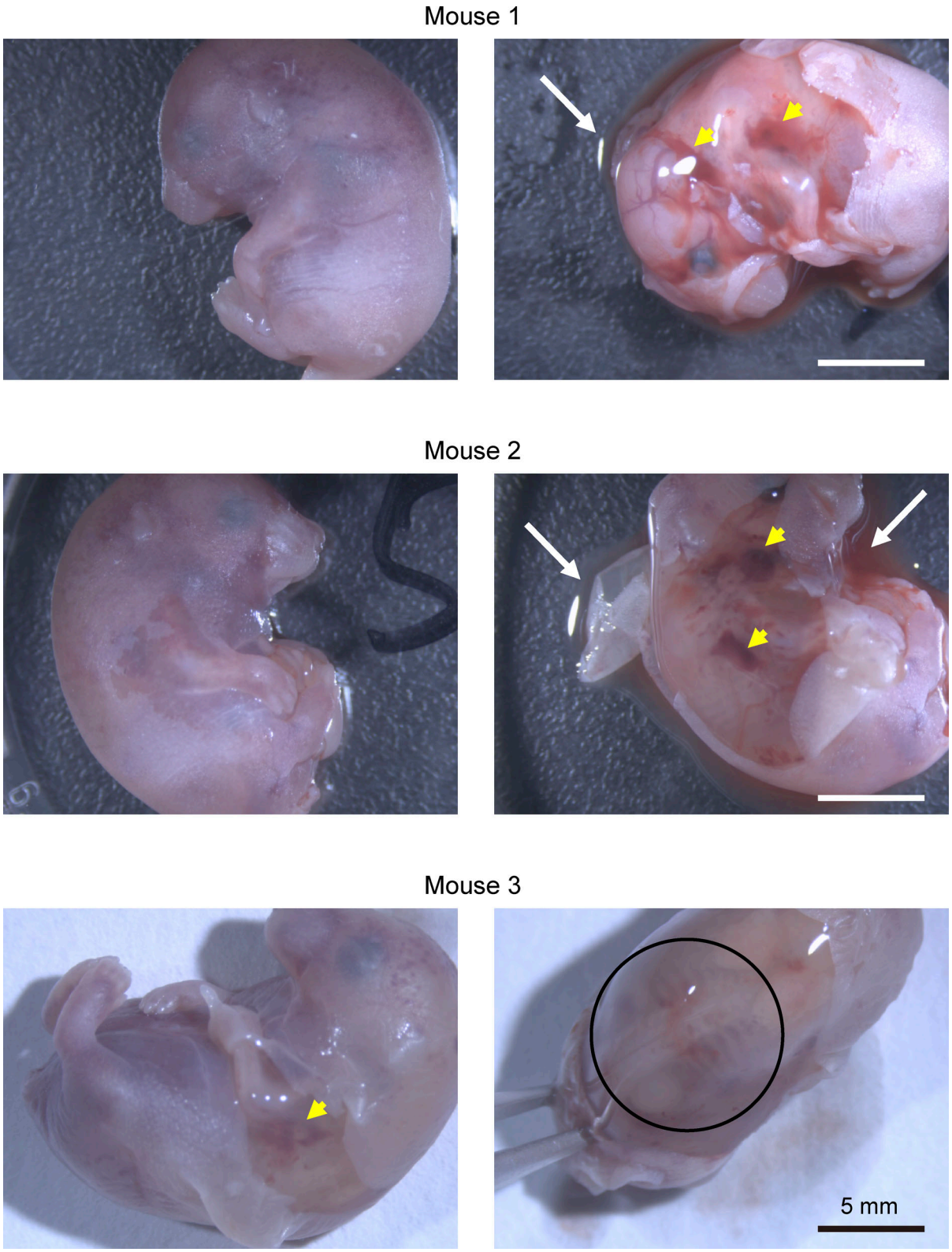

Figure S1. **Morphology of R2509C RYR1 homozygous embryos.** Three R2509C-Hom fetuses (E19–E20) were obtained from different heterozygous mothers. The fetuses showed abnormal death accompanied by subcutaneous hemorrhage (yellow arrows; mice 1–3), subcutaneous effusion (white arrows; mice 1 and 2), and translucent skeletal muscles (black line circle; mouse 3).

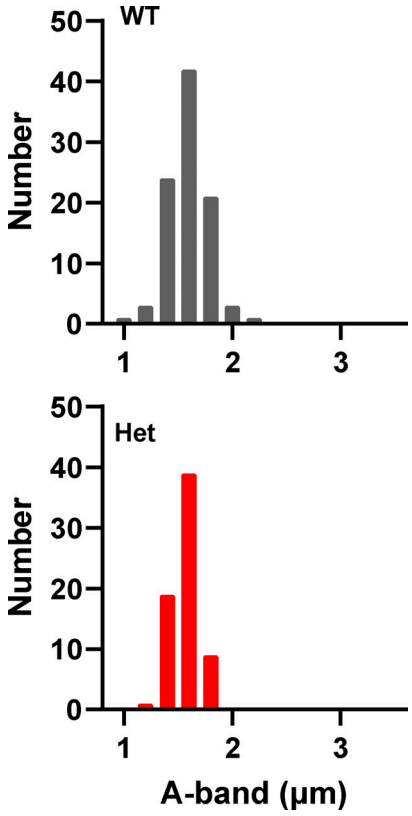

Figure S2. **Distribution of the lengths of A-band in WT and R2509C-Het primary myocytes.** The frequency histogram for A-band length in Fig. 2 C.

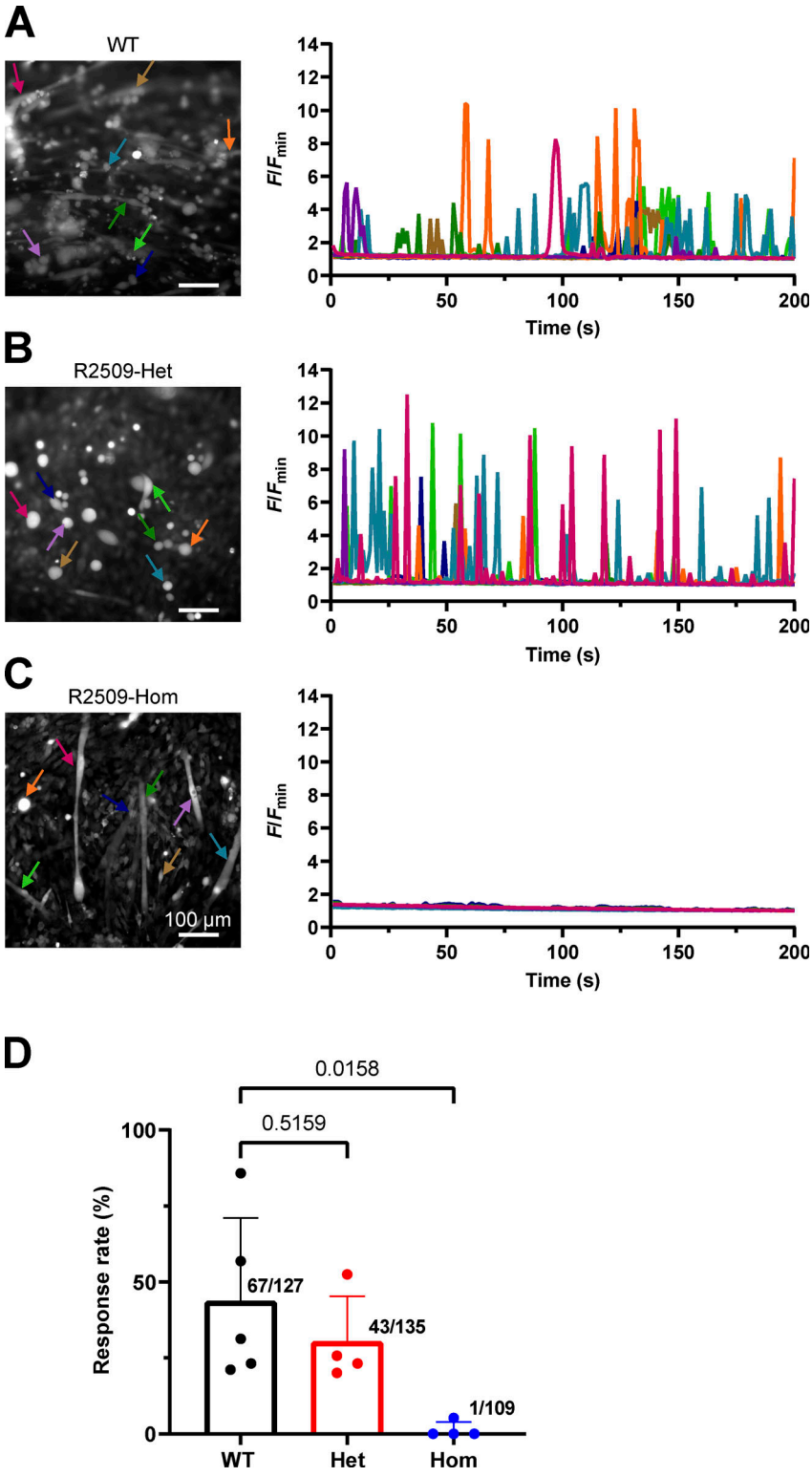

Figure S3. **Spontaneous Ca^{2+} transients in WT and R2509C mutant primary myocytes. (A–C)** Ca^{2+} transients in Cal-520–loaded primary myocytes at 3 d after differentiation from WT (A), R2509C-Het (B), and R2509C-Hom (C) mice were measured for 200 s with no stimulation. Different color lines indicate individual signals. Spontaneous Ca^{2+} transients were observed in primary myocytes from WT (Video 4) and R2509C-Het (Video 5) mice, but not in those from R2509C-Hom (Video 6) mice. **(D)** Number of myocytes demonstrating spontaneous Ca^{2+} transients out of total number of myocytes in the field of view during each observation, in which Ca^{2+} transients were measured for 200 s with no stimulation. The number at the top of bar indicates total number of positive myocytes out of total number of myocytes. Primary myocytes were cultured from three mice (N = 3) in each group (WT, R2509C-Het, and R2509C-Hom). Data are means ± SD (n = 4–5 observations) and analyzed by one-way ANOVA with Tukey's test.

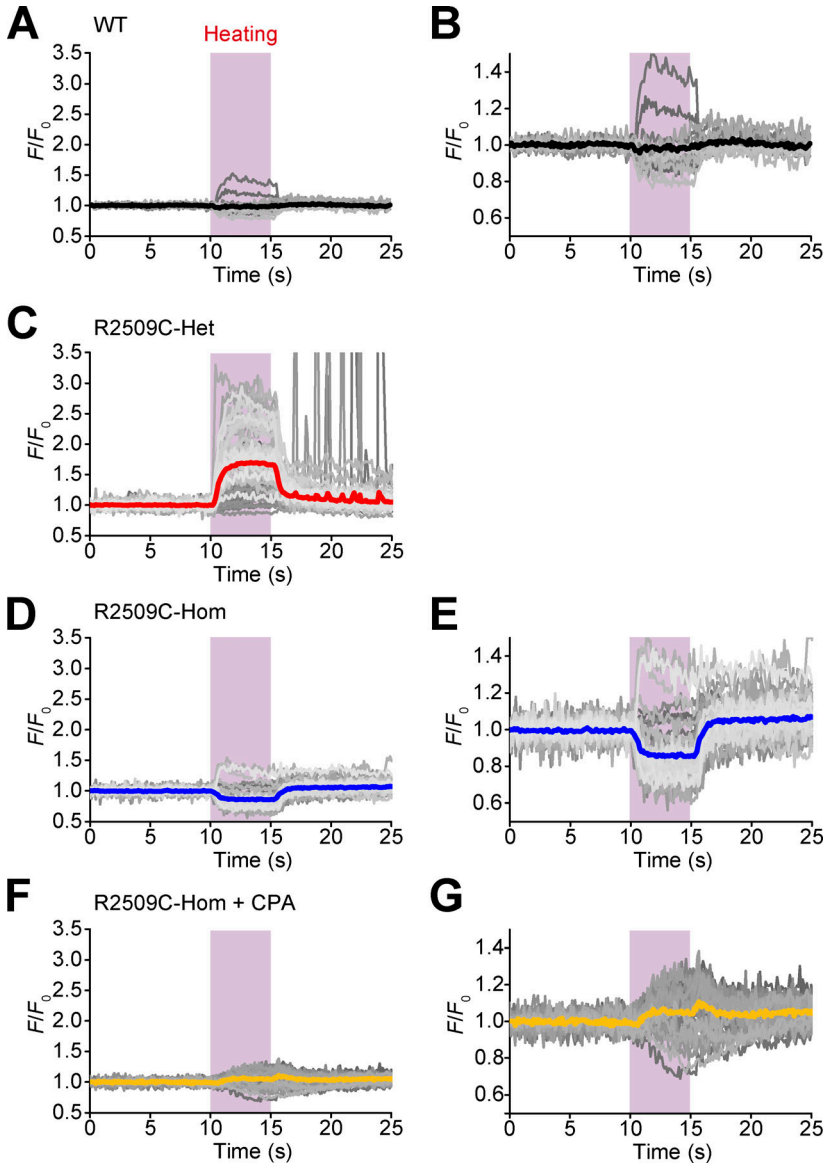

Figure S4. **Heat-induced Ca^{2+} release in WT and R2509C primary myocytes.** Time course of relative intensity of Cal-520–loaded primary myocytes from WT (A and B), R2509C-Het (C), R2509C-Hom (D and E), and R2509C-Hom + 20 µM CPA (F and G) mice. Figures in B, E, and G indicate enlarged images of A, D, and F, respectively.

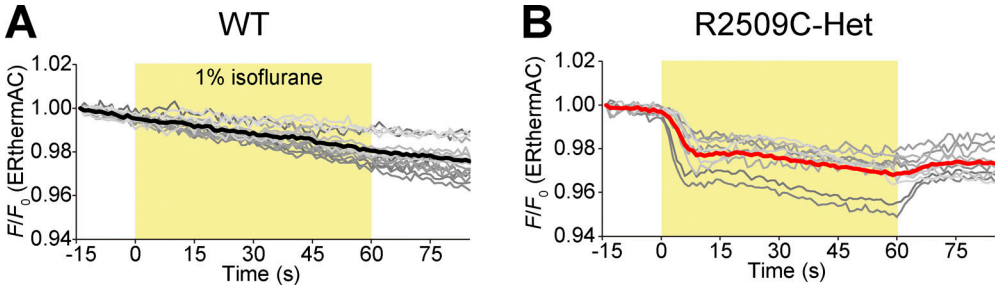

Figure S5. **Temperature measurement of the SR in FDB isolated skeletal cells during isoflurane application.** Time course of changes in the relative fluorescence intensity of ERthermAC in WT (A) and R2509C-Het (B) cells. Gray lines represent individual cells, and thick lines represent averages. Isoflurane (1%) was applied at the time points indicated by yellow horizontal bars.

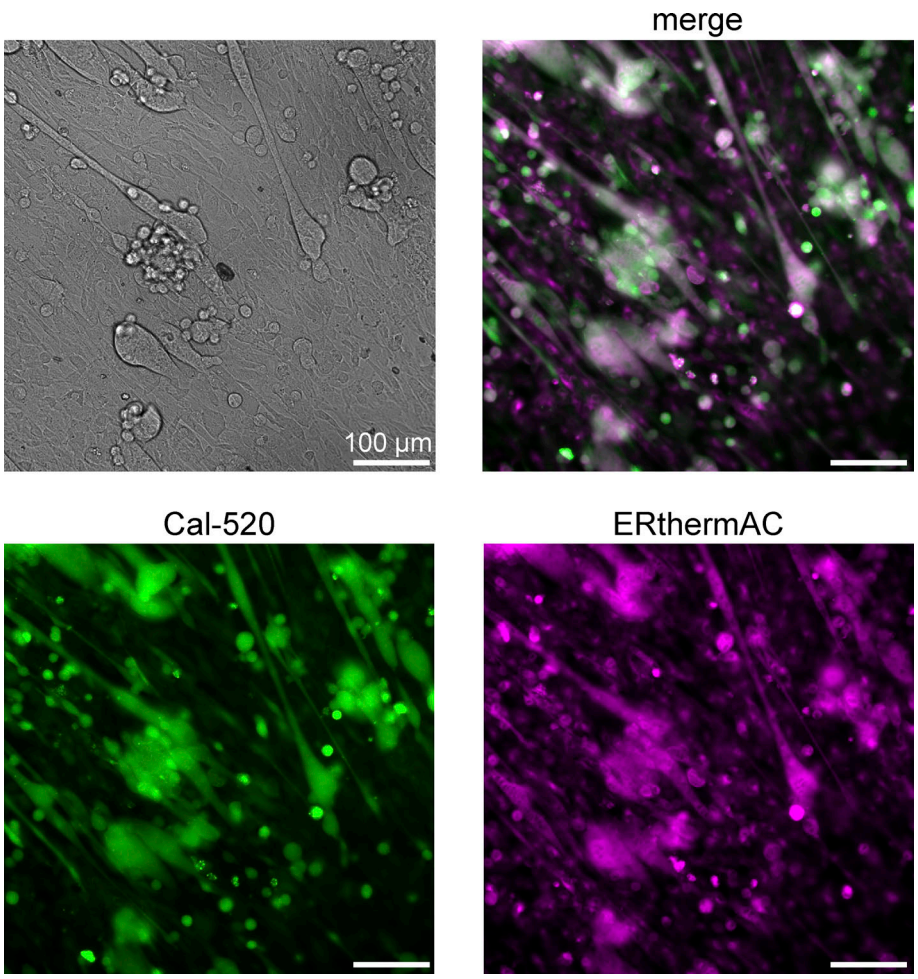

Figure S6. **ERthermAC staining in primary myocytes.** Representative images of bright-field (top left), and fluorescence images of WT primary myocytes co-stained with Cal-520 (bottom left) and the SR/ER-targeted fluorescent molecular thermometer ERthermAC (bottom right). Merged image is shown on the top right. Cal-520 was excited at 480 ± 9 nm, and fluorescence was imaged at 520 ± 14 nm. ERthermAC was excited at 556 ± 10 nm, and fluorescence was imaged at 617 ± 37 nm.

Video 1. **Spontaneous contraction in WT myocytes.** Transmission light microscopic images of WT myocytes. Scale bar, 100 µm. Playback speed, 1×.

Video 2. **Spontaneous contraction in R2509C-Het myocytes.** Transmission light microscopic images of R2509C-Het myocytes. Scale bar, 100 µm. Playback speed, 1×.

Video 3. **Spontaneous contraction in R2509C-Hom myocytes.** Transmission light microscopic images of R2509C-Hom myocytes. Scale bar, 100 µm. Playback speed, 1×.

Video 4. **Spontaneous Ca^{2+} transients in in WT myocytes.** Fluorescence microscopic images of Cal-520–loaded WT myocytes. Scale bar, 100 µm. Playback speed, 30×.

Video 5. **Spontaneous Ca^{2+} transients in R2509C-Het myocytes.** Fluorescence microscopic images of Cal-520–loaded R2509C-Het myocytes. Scale bar, 100 µm. Playback speed, 30×.

Video 6. **Spontaneous Ca^{2+} transients in R2509C-Hom myocytes.** Fluorescence microscopic images of Cal-520–loaded R2509C-Hom myocytes. Scale bar, 100 µm. Playback speed, 30×.